Monomeric structures of hexokinase I

by

Christina Ann Kirby

A thesis submitted to the graduate faculty

in partial fulfillment of the requirements for the degree of

MASTER OF SCIENCE

Major: Biochemistry

Major Professor: Richard B. Honzatko

Iowa State University

Ames, Iowa

1999

Graduate College

Iowa State University

This is to certify that the Master's thesis of

Christina Ann Kirby

has met the thesis requirements of Iowa State University

Signatures have been redacted for privacy

TABLE OF CONTENTS

CHAPTER 1. GENERAL INTRODUCTION 1

Introduction 1

Thesis Organization 5

References 6

CHAPTER 2. CRYSTAL STRUCTURES OF MUTANT MONOMERS OF RECOMBINANT HUMAN BRAIN HEXOKINASE REVEAL MULTIPLE ADP BINDING SITES AND CONFORMATIONAL CHANGES RELEVANT TO THE MECHANISM OF ALLOSTERIC REGULATION 8

Abstract 8

Introduction 9

Results and Discussion 11

Experimental 38

Acknowledgement 44

References 45

CHAPTER 3. GENERAL CONCLUSIONS 49

APPENDIX. ENTRAPMENT OF 6-THIOPHOSPHORYL-IMP IN THE ACTIVE SITE OF CRYSTALLINE ADENYLOSUCCINATE SYNTHETASE FROM ESHERICHIA COLI 51

CHAPTER 1. GENERAL INTRODUCTION

Introduction

Hexokinase catalyzes the conversion of glucose to glucose-6-phosphate (G6P) using adenosine triphosphate (ATP) as a phosphoryl donor. There are four isozymes of hexokinase, designated I-IV (1). Isozymes I-III have a molecular weight of 100,000 Daltons and are approximately 70% identical in their sequences (2). Furthermore, the N- and C-halves of isozymes I-III have significant sequence similarity. Isomer IV, commonly known as glucokinase, has a molecular weight of 50,000 Daltons and a sequence similar to those of N- and C-halves of isozymes I-III. This suggests the evolution of hexokinases I-IV from a primordial gene through duplication and fusion (3-6).

Although sequence similarity is strong among the four isozymes of hexokinase, their functional properties differ significantly. Hexokinase I, the focus of this study, has a catalytically active C-terminal half, whereas the N-terminal half functions solely as an allosteric domain (7,8). Both halves of hexokinase II, on the other hand, are catalytically active (9). Glucose 6-phosphate (G6P) inhibits both hexokinase I and II, but not glucokinase. Relief of G6P-inhibition by orthophosphate (P_i) only occurs in hexokinase I (7,10).

Hexokinase I controls the rate-limiting step of glycolysis both in the brain and red blood cell (11). The brain uses approximately 40% of all circulating glucose, consuming 13% of its weight in glucose daily, in order to support energy metabolism. Hexokinase I converts glucose into G6P, thereby trapping glucose in the cell and committing it to energy metabolism. An important property of hexokinase I is its low K_m value for glucose, which is 100 times lower than that of circulating glucose (5 mM). In order to prevent depleting the

entire supply of circulating glucose and compromising oxidative phosphorylation in the mitochondria, both G6P and P_i act as regulators of hexokinase I, with G6P acting as a potent feedback inhibitor and P_i relieving this inhibition. One molecule of glucose, G6P, or P_i can bind tightly to hexokinase I in the absence of ATP (12,13). Furthermore, the binding of G6P or P_i is synergistic with glucose.

For three decades, two mechanisms have been at the center of debate regarding allosteric regulation of hexokinase I. The first proposes that the G6P binds to the N-half (regulatory domain), inhibiting catalysis at the C-half (catalytic domain) (14). The alternative mechanism has G6P and ATP compete for the active site at the C-half (12). In both cases, P_i is thought to relieve G6P-inhibition by binding to an allosteric site in the N-terminal domain. When hexokinase I is cleaved into two halves, the isolated C-terminal half retains activity (7,15) and is still inhibited potently by G6P, but P_i relief of inhibition is lost (7,10,16). The isolated N-half is inactive but binds G6P tightly (7,17).

Recent crystal structures of hexokinase I, in combination with directed mutations, have led to yet another model for allosteric regulation of hexokinase I (18). Mutations were made in the G6P binding pocket of the N- and C-terminal halves of the enzyme, individually, with little effect on inhibition. The mutations were repeated on the genetically truncated C-terminal half, resulting in the complete loss of inhibition by G6P. Finally, double mutations were made in the N- and C-half binding sites for G6P of the full-length enzyme, which resulted in the complete loss of product inhibition. These data indicate both G6P binding sites can be or are functional.

Two structures of hexokinase I have been solved. The first structure shows glucose and G6P bound to both the N- and C-terminal halves of the enzyme and presents both halves

in what has been called the "closed" state (19). Each of the halves of hexokinase I is composed of two structural domains, called the large and small domains. In the closed conformation the small and large domains envelop active site ligands, whereas in the open conformation these domains are far apart, exposing the active site to solvent. In hexokinase I, the small subunit of the N-terminal half includes residues 75-209 and 448-465 while the large subunit is composed of residues 16-74 and 210-447. Residues 523-657 and 896-913 make up the small subunit of the C-terminal domain while the large subunit of this half includes residues 466-522 and 658-895. In the second structure, glucose and P_i are bound in the N-terminal domain while the C-terminal domain is unligated (20). The N-terminal domain exhibits the same closed conformation as seen in the previous structure, whereas the C-terminal domain remains in an "open" position. The difference between the open and closed conformation is a 17° rotation of the small domain with respect to the large domain.

Residues 448-475 of hexokinase I form a helix (hereafter called the transition helix), that connects the N- and C- halves. In addition, loop 242-253 of the N-terminal half and segment 796-813 of the C-terminal half interact by way of hydrogen bonds and non-bonded contacts. The non-bonded contacts between the N- and C-terminal halves may participate in the allosteric mechanism. In published crystal structures, hexokinase I is a dimer, assembled by interchain contacts between six different surface regions. Interactions in the G6P-complex involve three unique interfaces, referred to as the 1-6, 2-5, and 3-4 interfaces (Table 1), but the 2-5 interface is absent in the glucose/P_i-complex. In all complexes, however, the N- and C-halves of one subunit interact with the C- and N-halves, respectively, of the other subunit.

Table 1

Residue pairs involved in interchain or interdomain contacts less than 3.5 Å.

Interface name	Residue pair (glucose/Gluc-6-P structure)	Residue pair (glucose/P_i structure)
Interchain 1-6	Glu280- Lys558	Glu280- Lys558
	Arg283- Ile559[a]	Arg283- Ile559[a]
	Arg331[b]- Tyr588[a]	Arg283[a]-Ile559[b]
		Arg331[b]- Tyr588[a]
Interchain 2-5	Gly179[b]- Glu894	
Interchain 3-4	Asp54[a]- Gln894	Arg53[a]-Gln779
	Phe55[a]- Gln799	Asp54[a]-Gln806
	Thr58- Gln799	Pro57[a]-Gln789
Interdomain N-C	Asp251- Arg801	Asp251- Arg801
	Glu252- Arg801	Glu252- Cys813[b]
	Glu252- Cys813[b]	

[a] The backbone carbonyl group is involved in the interaction. [b] The backbone amide group is involved in the interaction.

Dimerization of hexokinase I is favored by either high protein concentration or by the presence of G6P (21). Small angle scattering experiments have shown that hexokinase I is a monomer in the presence of glucose and P_i at protein concentrations of up to 10 mg/ml, but in the presence of G6P the enzyme begins to form dimers at concentrations lower than 1 mg/ml. As the functional state of hexokinase I *in vivo* has yet to be determined, it is important to understand the effects of dimerization on enzyme structure and function. Directed mutations were made to the 1-6 interface of the wild-type enzyme with the intention of blocking dimerization. Small angle scattering experiments indicated that this mutant retained a rod-like monomeric conformation similar to that of a subunit in the dimer. Furthermore, regardless of protein and G6P concentration, the interface mutant remained as a monomer in solution. The interface mutant retained the kinetic properties of the wild-type enzyme, suggesting that observed functional properties of hexokinase I do not require aggregation to a dimer state.

It is known that hexokinase I associates with pores of the outer membrane of the mitochondria in some type of oligomeric form (22-25). Here it most likely interacts with a complex of proteins which work to shuttle ATP to hexokinase I and ADP to the matrix of the mitochondrion (26-28). G6P releases hexokinase I from the membrane, whereas ATP and Mg^{2+} promote membrane association of hexokinase I. The mechanism by which ligands modulate the binding of hexokinase I to the mitochondrial membrane is unclear, but in the crystal structure presented in this thesis a new adenine binding site to the regulatory domain is observed. This adenine binding site is proximal to structural elements putatively essential to hexokinase I association with the mitochondrial membrane, and hence could represent an additional regulatory site for enzyme-membrane association.

Thesis Organization

This thesis is composed of two manuscripts. The first is entitled "Crystal Structures of Mutant Monomers of Recombinant Human Hexokinase Reveal Multiple ADP Binding Sites and Conformational Changes Relevant to the Mechanism of Allosteric Regulation" and involves an enzyme that is the focus of my current research. This manuscript is, therefore, included in this thesis as a chapter. The paper presents monomeric forms of hexokinase I for the first time, gives insight as to how ADP binds to the active site, reveals an additional binding site for ADP, and provides a structural basis for allosteric regulation of catalysis. My contributions to this work included purification of the quadruple mutant and consequent crystallization of this mutant with ADP. I also participated in data collection (Argonne synchrotron) and contributed significantly to the writing of the manuscript for submission to the *Journal of Molecular Biology*.

I have also included a paper that was published in the *Journal of Biological Chemistry* in June 1997 entitled "Entrapment of 6-Thiophosphoryl-IMP in the active site of Crystalline Adenylosuccinate Synthetase from *Esherichia coli*." My contributions to this work included purification of adenylosuccinate synthetase and consequent crystallization of this enzyme. I also assisted in the data collection and worked to refine the structure. This is added as an appendix since it still pertains to my specialization, x-ray crystallography, but focuses on a different enzyme from that in the body of the thesis.

References

1. Katzen, H. M. & Schimke, R. T. (1965) *Proc. Natl. Acad. Sci. U.S.A.* **54**, 1218-1254.
2. Wilson, J. E. (1995) *Rev. Physiol. Biochem. Pharmacol.* **126**, 65-198.
3. Easterby, J. S. & O'Brien, M. J. (1973) *Eur. J. Biochem.* **38**, 201-211.
4. Holroyde, M. J. & Trayer, I. P. (1976) *FEBS Lett.* **62**, 215-219.
5. Ureta, T. (1982) *Comp. Biochem. Physiol. B: Comp. Biochem.* **71**, 549-555.
6. Manning, T. A. & Wilson, J. E. (1984) *Biochem. Biophys. Res. Commun.* **118**, 90-96.
7. White, T. K. & Wilson, J. E. (1989) *Arch. Biochem. Biophys.* **274**, 375-393.
8. Arora, K. K., Filburn, C. R. & Pedersen, P. L. (1993) *J. Biol. Chem.* **266**, 5359-5362.
9. Tsai, H. J. & Wilson, J. E. (1996) *Arch. Biochem. Biophys.* **329**, 17-23.
10. Zeng, C. & Fromm, H. J. (1995) *J. Biol. Chem.* **270**, 10509-10513.
11. Lowry, O. H. & Passonneau, J. V. (1964) *J. Biol. Chem.* **239**, 31-42.
12. Ellison, W. R., Lueck, J. D. & Fromm, H. J. (1975) *J. Biol. Chem.* **250**, 1864-1871.
13. Mehta, A., Jarori, G. K. & Kenkare, U. W. (1988) *J. Biol. Chem.* **263**, 15492-15497.
14. White, T. K. & Wilson, J. E. (1987) *Arch, Biochem. Biophys.* **259**, 402-411.

15. Arora, K. K., Filburn, C. R., & Pedersen, P. L. (1991) *J. Biol. Chem.* **266** 5359-5362.

16. Magnani, M., Bianchi, M., Casabianca, A., Stocchi, V., Daniele, A., Altruda, F., Ferrone, M. & Silengo, L. (1992) *Biochem. J.* **285**, 193-199.

17. Arora, K. K., Filburn, C. R. & Pedersen, P. L. (1993) *J. Biol. Chem.* **268**, 18259-18266.

18. Liu, X., Kim, C. S., Kurbanov, F. T., Honzatko, R. B. & Fromm, H. J. (1999) *J. Biol. Chem.*, submitted.

19. Aleshin, A. E., Zeng, C., Bourenkov, G. P., Bartunik, H. D., Fromm, H. J. & Honzatko, R. B. (1998) *Structure* **6**, 39-50.

20. Aleshin, A. E., Zeng, C., Bartunik, H. D., Fromm, H. J. & Honzatko, R. B. (1998) *J. Mol. Biol.* **282**, 345-357.

21. Aleshin, A. E., Malfois, M., Liu, X., Kim, C. S., Fromm, H. J., Honzatko, R. B., Koch, M. H. J. & Svergun, D. I. (1999) *Biochemistry* **38**, 8359-8366.

22. Beutner, G., Rück, A., Riede, B., Welte, W. & Brdiczka (1996) *FEBS Lett.* **396**, 189-195.

23. Beutner, G., Rück, A., Riede, B. & Brdiczka (1997) *Biochem. Soc. Trans.* **25**, 151-157.

24. Beutner, G., Rück, A., Riede, B. & Brdiczka (1998) *Biochim. Biophys. Acta.* **1368**, 7-18.

25. Xie, G. & Wilson, J. E. (1990) *Arch. Biochem. Biophys.* **276**, 285-293.

26. Wicker, U., Bücheler, K., Gellerich, F. N., Wagner, M., Kapischke, M. & Brdiczka, D. (1993) *Biochim. Biophys. Acta.* **1142**, 228-239.

27. Rose, I. A. & Warms, J. V. B. (1967) *J. Biol. Chem.* **242**, 1635-1645.

28. de Cerqueira Cesar, M. & Wilson, J. E. (1998) *Arch. Biochem. Biophys.* **350**, 109-117.

CHAPTER 2. CRYSTAL STRUCTURES OF MUTANT MONOMERS OF RECOMBINANT HUMAN BRAIN HEXOKINASE REVEAL MULTIPLE ADP BINDING SITES AND CONFORMATIONAL CHANGES RELEVANT TO THE MECHANISM OF ALLOSTERIC REGULATION

A paper submitted to the Journal of Molecular Biology

Alexander E. Aleshin, Xiaofeng Liu, Christina Kirby, Gleb P. Bourenkov, Hans D. Bartunik, Herbert J. Fromm, and Richard B. Honzatko

Abstract

Hexokinase I, the pacemaker of glycolysis in brain tissue, is composed of two structurally similar halves connected by an α-helix. The enzyme dimerizes at elevated protein concentrations in solution and in crystal structures; however, almost all published data reflect the properties of a hexokinase I monomer in solution. Crystal structures of mutant forms of recombinant human hexokinase I, presented here, reveal the enzyme monomer for the first time. The mutant hexokinases bind both glucose 6-phosphate and glucose with high affinity to their N- and C-terminal halves, and ADP, also with high affinity, to a site near the N-terminus of the polypeptide chain. Exposure of the monomer crystals to ADP in the complete absence of glucose 6-phosphate reveals a second binding site for adenine nucleotides at the putative active site (C-half), with conformational changes extending 15 Å to the contact interface between the N- and C-halves. The structures reveal a

flexible region of the C-half and a rigid-body rotation of the N-half, as possible elements of a structure-based mechanism for allosteric regulation of catalysis.

Introduction

Hexokinase I (ATP: D-hexose 6-phosphotransferase, EC 2.7.1.1) governs the flow of glucose into the energy metabolism of the brain and the red blood cell (1). The type I isozyme, one of four hexokinase isozymes found in mammals (2), is a single polypeptide of molecular mass 100 kDa. The N- and C-terminal halves of hexokinase I are similar in sequence (3,4) and in structure (5-8). The sequence similarity putatively stems from the duplication and fusion of a primordial hexokinase gene (9-12). Hexokinase I uses ATP to phosphorylate the 6-hydroxyl group of glucose (Glc) and is inhibited potently by the product, glucose 6-phosphate (G6P). Hexokinase I is distinct from hexokinase isozymes in that orthophosphate (P_i) at physiological levels can relieve inhibition by G6P (13-15).

The N-half of hexokinase I has no catalytic activity (16,17). It does have, however, a high-affinity binding site for P_i, responsible for the relief of G6P inhibition (6,18) and a high affinity binding site for G6P, which causes allosteric inhibition of hexokinase I (19,20). The C-terminal half is catalytically active (16,21). As an isolated domain, the C-terminal half is inhibited potently by G6P, but lacks the property of P_i-induced relief of product inhibition (16,22,23). Furthermore, the high-affinity binding site for G6P at the C-half is functional in some mutants of the full-length enzyme (18,20). Hence, mechanisms of allosteric inhibition and direct competition for the active site by G6P operate in hexokinase I. In equilibrium binding experiments, the full-length enzyme binds one molecule of Glc, G6P or P_i tightly in the absence of ATP (14,24). G6P and Glc bind synergistically to hexokinase I, as do Glc and

P_i (24). The observation of two high-affinity binding sites for G6P, one each in the N- and C-half, but a binding stoichiometry of one G6P molecule per hexokinase subunit, suggests a mechanism of anti-cooperativity in the binding of G6P (20).

At concentrations below 10 μg/ml of enzyme, typical for kinetics investigations, hexokinase I is a monomer (25,26). At enzyme concentrations above 10 mg/ml, hexokinase I aggregates, and is a dimer in all crystal structures (5-8). The extent to which dimerization of hexokinase I perturbs the conformation of the monomer is unclear. Small angle X-ray scattering data from solutions of the wild-type enzyme and a triple mutant of hexokinase I, designed specifically to block subunit dimerization, however, indicate a rod-like conformation for the monomer, similar to that observed for the subunit in crystal structures (26).

Here we present the first crystal structures of hexokinase I as a monomer. We have employed a triple mutant of the recombinant human enzyme (Glu280→Ala, Arg283→Ala, and Gly284→Tyr), which does not dimerize, even at concentrations as high as 16 mg/ml, and yet quantitatively retains all of the kinetic properties of wild-type hexokinase I (26). The new crystal form of the monomer requires ADP and G6P for its growth, and diffracts to 1.9 Å resolution. The high resolution data from this crystal form, nearly 1 Å better than any other published structure of hexokinase I, has revealed an error in orientation of the pyranose moiety of bound G6P (5). Also revealed is a high-affinity binding site for ADP near the N-terminus of the hexokinase I polypeptide chain. As G6P binds with such high affinity to crystals of this triple mutant, we produced and functionally characterized an additional quadruple mutant of hexokinase I (Glu280→Ala, Arg283→Ala, Gly284→Tyr, and Thr536→Ala), which in solution lacks the high-affinity binding site for G6P at the C-half.

When crystals of the quadruple mutant are soaked in ADP solutions, purged of all traces of G6P, a second molecule of ADP binds to the putative active site of the C-half. Conformational changes in response to ADP association with the C-half extend 15 Å to the contact interface between the N- and C-halves of the monomer. The analysis of conformational differences over all available crystal structures of hexokinase I suggests that a rigid-body rotation of the N-terminal half may couple with the observed conformational changes in the C-half. Hence, the state of ligation of the N-half may be relayed to the adenine binding pocket of the C-half by way of the intrasubunit contact interface.

Results and Discussion

Functional properties and state of ligation of mutant hexokinases— The crystal structures of two mutant forms of hexokinase I are presented here, the first mutants of a mammalian hexokinase to be examined by X-ray diffraction. The combined mutations of Glu280→Ala, Arg283→Ala, and Gly284→Tyr block dimerization of hexokinase I subunits at high concentration (26). Furthermore, the triple mutant has functional properties that are quantitatively indistinguishable from those of the wild-type enzyme (Table 1). The triple mutant crystallizes as a monomer in the space group $P2_12_12$ with unit cell parameters a=145.66, b=145.80, and c=58.13 Å and diffracts to 1.9 Å resolution. A second mutant of hexokinase I, combines the three mutations above along with the mutation of Thr536 to alanine. The mutation at position 536 eliminates high affinity binding of G6P to the C-half of hexokinase I, as evidenced by its effect on the truncated C-half of hexokinase I (Table 1). Otherwise the quadruple mutation of hexokinase I has little or no effect on kinetic parameters, except for a 7-fold decrease in k_{cat}, indicating a modest destabilization of the

Table 1
Kinetic Parameters for Wild-Type and Mutant Hexokinases.

Enzyme (%)	k_{cat} (s^{-1})	K_M^{ATP} (mM)	K_M^{Glc} (μM)	K_i[e] (μM)	P_i-relief[f] (%)
WT[a]	60.9±5.3	0.44±0.07	41±1.9	18.2±2.2	72±6
Triple[b]	72.1±4.0	0.66±0.07	29.4±3.9	21.2±1.8	80±6
Quadruple[c]	10.5±1.0	1.58±0.05	44.9±3.5	11.3±0.37	85±6
T536A-mini[d]	44.0±4.8	0.37±0.03	56.8±2.9	N.D.[g]	N.D.[g]

[a] Wild-type hexokinase I. [b] Triple (E280→A, R283→A, G284→Y) mutant of hexokinase I. [c] Quadruple (E280→A, R283→A, G284→Y, T536→A) mutant of hexokinase I. [d] T536A mutant of truncated C-half (residues 455-917) of hexokinase I. [e] K_i was obtained from plots of 1/velocity versus 1/[ATP] at 2 mM glucose with 1,5-AnG6P ranging from 0 to 400 μM. [f] Percent relief of 1,5-AnG6P inhibition by P_i was determined as follows: $100 \times (A - B)/A$, where A is the slope from the plot of (relative velocity of hexokinase)$^{-1}$ *versus* 1,5-AnG6P concentration in the absence of P_i and B is the slope from the plot of (relative velocity of hexokinase)$^{-1}$ *versus* 1,5-AnG6P concentration in the presence of 6 mM P_i. [g] Not detectable.

transition state. Crystals of the quadruple mutant are isomorphous to those of the triple mutant and diffract to the same limit.

For reasons presented below, both triple and quadruple mutant enzymes require ADP and G6P for crystal growth. The triple mutant grows in as little as 45 μM G6P, whereas the quadruple mutant requires G6P concentrations of 20 mM. In crystals grown under these conditions both the triple and quadruple mutant enzymes have G6P and Glc bound to their C- and N-halves. G6P present in the initial crystallization experiment of the triple mutant (Table 2, column 1) results from the phosphorylation of Glc by the triple mutant, using the ATP, present as a contaminant of the ADP reagent (see Experimental section). Although the estimated concentration of G6P was less than 45 μM (~4 K_d) and that of ADP was 25 mM (~12 K_d), G6P saturates the N-half of the crystal represented by Table 2, column 1, and nearly saturates the C-half (75% occupancy). We observe electron density at the C-half in the adenine-binding pocket, which could represent low occupancy (25%) of the ADP site. Increasing the concentration of G6P to 0.6 mM saturates both the N- and C-halves in crystals

Table 2

Statistics from data collection and refinement.

Protein	Triple Mutant[a]	Triple Mutant[a]	Quadruple Mutant[b]	Quadruple Mutant[b]
Soaking Conditions	ADP(ATP), Mg^{2+}, Glc, AlF_4	G6P, Glc	ADP(pure), Mg^{2+}, Glc, 1.5 hours	ADP(pure), Mg^{2+}, Glc, 5 hours
Wavelength (Å)	1.05	1.05	1.00	1.00
Distance to detector (mm)	100	110	270	250
Resolution (Å)	1.9	2.0	2.7	2.8
No. of reflections collected	454,280	286,697	133,320	65,575
No. of unique reflections	96,631	83,349	30,082	25,491
% Completeness	98.3	98.6	86.6	77.5
R_{merge}[c]	0.055	0.048	0.052	0.064
% Completeness (last shell)	98.3	82.3	50.1	57.0
R_{merge}[c] (last shell)	0.55	0.41	0.18	0.44
Resolution of refinement (Å)	8.0-1.9	8.0-2.0	8.0-2.7	8.0-2.8
R-factor[d]	0.211	0.211	0.225	0.260
R_{free}[e]	0.258	0.268	0.283	0.310
No. atoms in refinement	7,822	7,897	7,501	7,263
No. waters	682	706	307	102
Root mean squared deviations(Å):				
Bond distance (sigma)	0.015 (0.02)	0.016 (0.02)	0.011 (0.02)	0.010 (0.02)
Angle 1-3 distance (sigma)	0.033 (0.04)	0.036 (0.04)	0.039 (0.04)	0.039 (0.04)
Torsion 1-4 distance (sigma)	0.036 (0.05)	0.038 (0.05)	0.043 (0.05)	0.040 (0.05)

Table 2
(continued)

Mean B factors ($Å^2$):				
Protein from refinement	35.3	39.0	33.2	50.6
From Wilson plot	30.6	33.2	35.0	50.6
Glucose, N-domain	19.8	25.1	16.1	35.0
Glucose, C-domain	19.9	23.1	16.2	33.7
G6P, N-domain (occupancy[f])	22.4 (1.0)	26.0 (1.0)	14.1 (0.35)	-[g]
P_i, N-domain (occupancy[f])	-[g]	-[g]	19.4 (0.65)	39.7 (1.00)
G6P, C-domain (occupancy[f])	22.7 (0.7)	26.6 (1.0)	13.4 (0.35)	-[g]
ADP, C-domain (occupancy[f])	- (0.3[h])	-[g]	67.9 (0.65)	74.1 (1.00)
ADP, N-domain (occupancy[f])	34.3 (1.0)	39.6 (0.6)	46.1 (1.0)	48.5 (1.0)

[a] Hexokinase I with mutations Glu280→Ala, Arg283→Ala, Gly284→Tyr. [b] Hexokinase I with mutations Glu280→Ala, Arg283→Ala, Gly284→Tyr, Thr536→Ala. [c] $R_{merge} = \Sigma_i\Sigma_j |I_{ij} - \langle I_j \rangle| / \Sigma_i\Sigma_j I_{ij}$. [d] R-factor = $\Sigma ||F_{obs}| - |F_{calc}|| / \Sigma |F_{obs}|$, for all reflections $|F_{obs}| > 0$. [e] R-factor based on 5% of the data excluded from refinement. [f] Obtained by trial-and-error adjustment during refinement. [g] Not bound. [h] Estimated value.

of the triple mutant (Table 2, column 2). G6P binds weakly to the C-half of the quadruple mutant in solution (Table 1), necessitating an elevated concentration of G6P for crystallization. Yet unpurified ADP is ineffective in displacing G6P from crystals of the quadruple mutant. A crystal of quadruple mutant, soaked for 24 hours in 50 mM of unpurified ADP, followed by soaking for 1.5 hours in 100 mM of purified ADP (see Experimental section) retained approximately 35% of its bound G6P molecules (Table 2,

column 3). Evidently, once locked by lattice contacts into a conformation favorable for G6P-binding, the affinity of G6P for the N- and C-halves is high, and the mutation at position 536 has little influence. Only after 5 hours of soaking in 100 mM of purified ADP could we eliminate G6P from the N- and C-halves of the quadruple mutant (Table 2, column 4). The specimens represented by Table 2, columns 3 & 4, have ADP at the C-half and P_i at the N-half. Inorganic phosphate was not added to the system, but probably arises from the ADP reagent, either as a contaminant or as a breakdown product.

Hereafter, we will refer to the structure of G6P/Glc complex of the triple mutant (Table 2, columns 1 & 2) as G6Pm (G6P-monomer) and the structure of ADP/Glc complex of the quadruple mutant (Table 2, columns 3 & 4) as ADPm (ADP-monomer). By analogy then, the crystal structure of the hexokinase I dimer complexed with P_i and Glc (6) is P_id (P_i-dimer) and that of hexokinase I complexed with G6P and Glc (5) is G6Pd (G6P-dimer).

General attributes of G6Pm and ADPm— Statistics from data collection and refinement are in Table 2. The asymmetric unit is one polypeptide chain of hexokinase I, which occupies 46% of the total volume. As in previous structures of the hexokinase I dimers (5-8) the first 15 and the last 2 residues are not evident in electron density maps of G6Pm and ADPm. At both ends of the polypeptide chain thermal parameters rise to approximately 100 $Å^2$. On the basis of PROCHECK (27), all structural parameters are within (or better than) those of an "average" structure of comparable resolution. Only 2 out of 898 residues fall into generously allowed regions of the Ramachandran plot. Estimates of the overall root mean square error in atom positions (28) are 0.16 Å for the high resolution structures (G6Pm) and 0.45 Å for the lower resolution structures (ADPm). As in structures of the previously reported dimers, loop 98-104 has high thermal parameters. The crystal

structures of hexokinase I with the interface mutations have an additional area in the C-domain (residues 793-813) where thermal parameters are high (about 100 $Å^2$). This area consists of a helix and two loops (Figs. 1 & 2), which may play a central role in the mechanism of allosteric regulation of catalysis. In G6Pm (G6P occupancy 100% in both the N- and C-half as in Table 2, column 2) the electron density for this area matches that of G6Pd and P_id in the corresponding region. Hence, here we fit and refined the structure of the G6P/Glc-dimer. The electron density in ADPm differed significantly from that of G6Pm for residues 792-798; however, the weak density here complicated model building. Nonetheless the main chain of loop 792-798 falls into the electron density with torsion angles in the allowed regions of the Ramachandran plot. Moreover, yeast hexokinase complexed with Glc has a similar conformation of the corresponding loop (29). Although side chains are in the model for loop 792-798, they have little or no associated electron density.

Global structure of hexokinase I in G6Pm and ADPm— Even though contacts between molecules in G6Pm and ADPm are completely different from those of G6Pd and P_id, all of the polypeptide chains of hexokinase I have similar, rod-like conformations, in agreement with results from small angle X-ray scattering experiments (26). X-ray scattering curves from solutions of wild-type and triple-mutant forms of hexokinase I are consistent with the structures of crystallographic dimers and the rod-like subunits observed in crystal structures. Hence, the interface responsible for relaying the allosteric signal from the N- to C-half probably involves structural elements identified previously in G6Pd and P_id, namely loop 249-252 of the N-half and residues 801 and 813 of the C-half (5,6,18). In G6Pm and ADPm, however, the N- and C-halves interact only through the connecting helix (hereafter called the transition helix); the non-covalent interactions between halves, observed in dimer

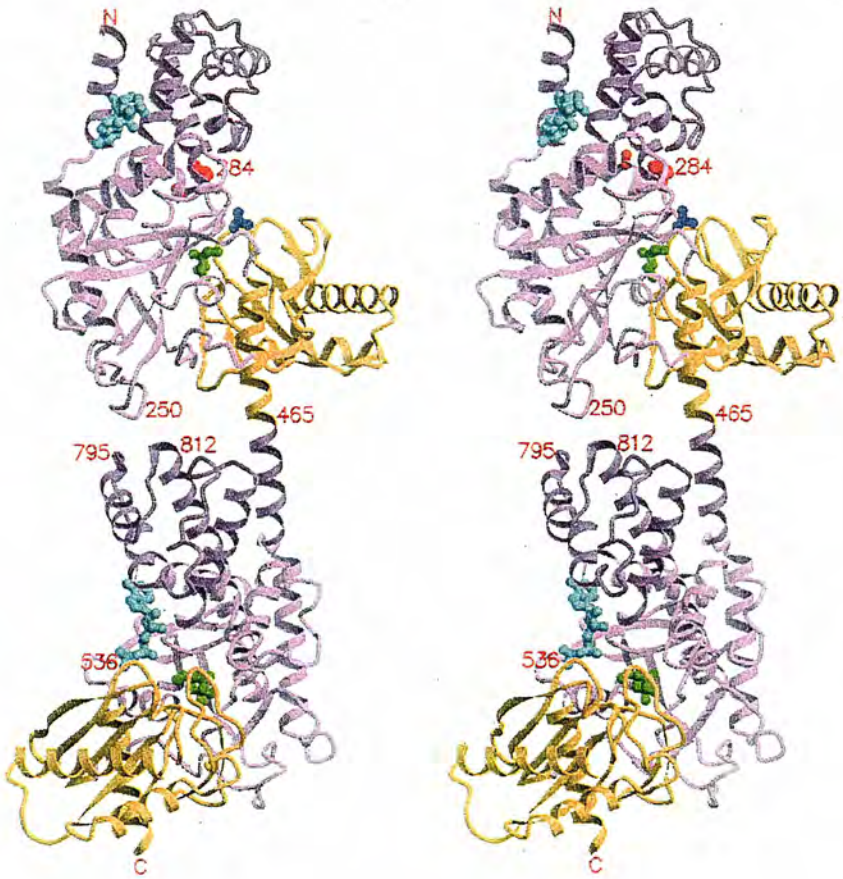

Figure 1. Stereoview of the hexokinase I monomer. The large and small domains of the N- and C-halves are shown in purple and yellow, respectively. The variable subdomain of the large domain, which includes the flexible loop 795-812, is shown in dark purple. The side chains of residues 281, 283, and 284, which were altered by mutation to block dimerization, are in red. ADP molecules are in blue, glucose molecules are green and the phosphate molecule bound only to the N-half is blue. Illustrated here is the structure presented in Table 2, column 4. This drawing was made with MOLSCRIPT (30) and RASTER3D (31).

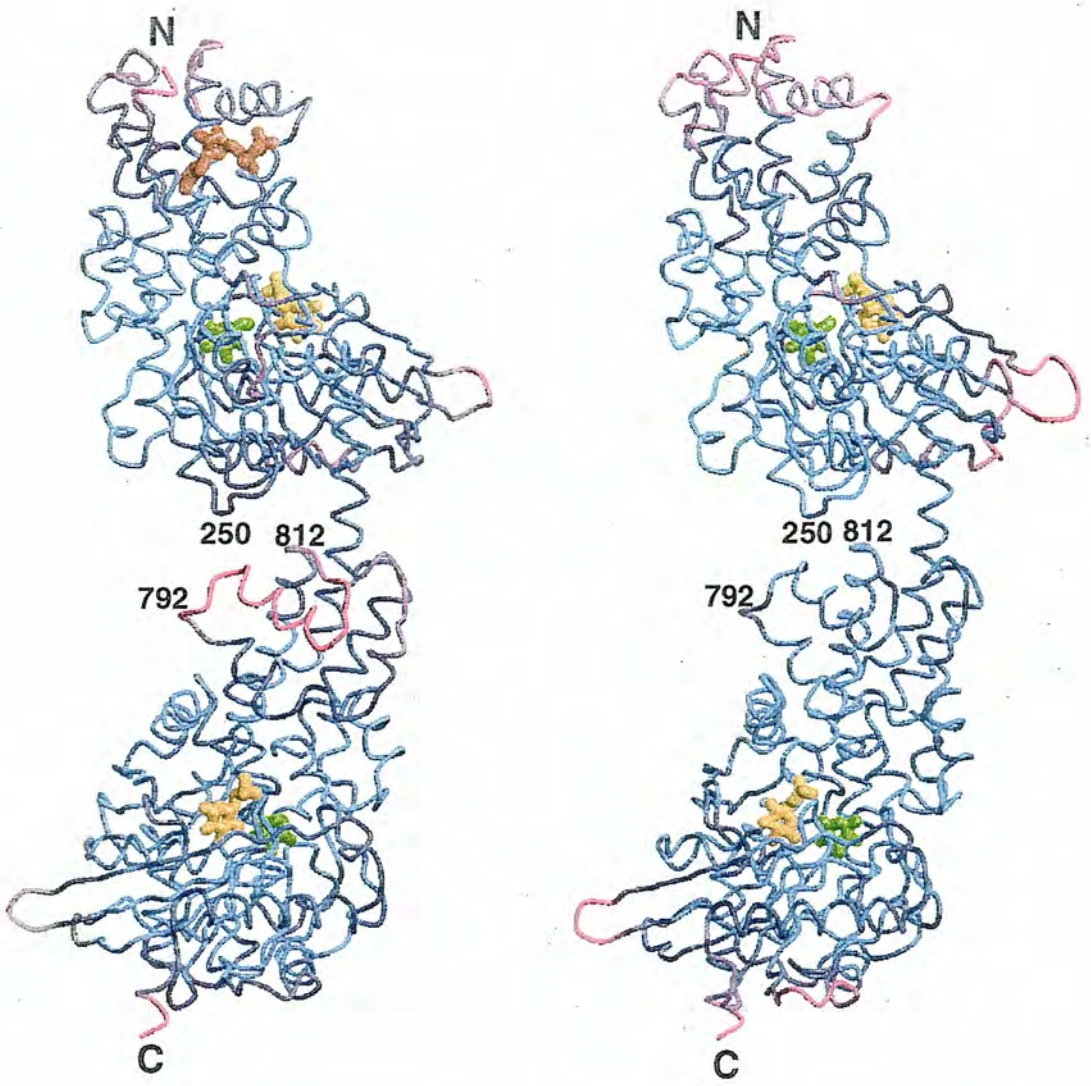

Figure 2. Conformations and thermal parameters of hexokinase I monomer. (A) Structure from Table 2, column 2, with G6P in yellow, glucose in green and ADP in brown. (B) Chain B of G6Pd (PDB entry 1HKB) with G6P in yellow and glucose in green. The thermal parameters of the main chain are coded by color varying from blue (thermal parameters of 30Å^2) to red (thermal parameters of 90 Å^2). The significance of high thermal parameters in the flexible element (residues 792-812) is discussed in the text. This drawing was made with MOLSCRIPT (30) and RASTER3D (31).

in structures, are absent. Evidently the two halves of the triple and quadruple mutants in G6Pm and ADPm are decoupled, which may account for G6P binding to both halves of the molecule. This view is consistent with recent experiments in kinetics, which indicate one high affinity site each for G6P at the N- and C- terminal halves, both of which cause potent inhibition of catalysis (20). The binding of G6P to these sites occurs putatively with negative cooperativity, so that in a coupled monomer, the fractional occupancy for G6P in the two sites should sum to unity. In the crystal structure of G6Pm, however, we observe full occupancy for both G6P-sites. Either lattice contacts and/or the conditions of crystallization by themselves stabilize a decoupled conformer.

Rigid-body conformational changes within the N- and C-halves of hexokinase I structures— A systematic comparison of the C-halves of P_id and G6Pd reveals a 17±2°-rotation of the small domain relative to the large domain [Fig. 1, (6)]. This relative movement of the small domain distinguishes the open from the closed conformation of the C-half of hexokinase I. In G6Pm and G6Pd the small and large domains have the same relative orientation and position (closed conformation). The large domain also has a subset of residues (hereafter called the variable subdomain), which move as a rigid body with respect to the rest of the large domain (the invariant portion, Fig. 1 & Table 3). A small deformation (bend) in helix α11 (residues 812-849) causes nearly a 4° rotation of the variable subdomain in the closed relative to the open C-half. The relative rotations of variable subdomains for closed C-halves from different crystal forms are smaller (Table 3) and may arise from differences in lattice contacts. The structures of G6Pm and ADPm reveal a very variable element (residues 793-813) within the variable subdomain of the C-half. The significance of this flexible element to ADP binding and allosteric regulation of catalysis is discussed below.

Table 3

Rigid body rotations and root mean square deviations (rmsd) of domains in P_id, G6Pd, and G6Pm.

Element compared or used as a basis of superposition	Additional rotation to superimpose compared elements (rmsd in Å of Cα atoms for superimposed elements)		
	P_id vs. G6Pd	P_id vs. G6Pm	G6Pd vs. G6Pm
Variable subdomain of N-half[b,d]	0.8° (0.40)	1.4° (0.35)	1.3° (0.44)
Small domain of N-half[b,e]	2.8° (0.39)	1.3° (0.37)	1.6° (0.32)
Invariant part of N-half[c,f]	(0.31)	(0.44)	(0.34)
Variable subdomain of C-half[b,g]	3.9° (0.34)	3.2° (0.48)	2.0° (0.43)
Small domain of C-half[b,h]	17.5° (1.0)	16.8° (1.0)	2.2° (0.36)
Invariant part of C-half[c,i]	(0.43)	(0.46)	(0.42)
N-half[b,j] Large domain of C-half[c,k]	21.6°	26.0°	13.0°
N-terminus of transition helix[b,l] C-terminus of transition helix[c,m]	16.7°	15.7°	10.5°
N-half[b,j] N-terminus of transition helix[c,l]	8.1°	6.3°	2.1°
Large domain of C-half[b,k] C-terminus of transition helix[c,m]	7.5°	8.5°	4.0°

[a] For each pair of structures as element is chosen as a basis of initial superposition. The angle represents an additional rotation necessary to superimpose the compared elements after the application of the rigid-body transformation used to bring about the superposition of the basis elements. Residues at the ends of elements, which deviate significantly from rigid body movements, were excluded from calculations. [b] Compared structural element. [c] Element used as a basis for the initial superposition. [d] Residues 16-30 and 302-382. [e] Residues 30-73, 209-302, and 381-449. [f] Residues 73-209 and 451-465. [g] Residues 466-478 and 750-829. [h] Residues 478-521, 657-750, and 829-895. [i] Residues 521-657 and 895-913. [j] Residues 16-465. [k] Residues 466-521 and 657-895. [l] Residues 452-462. [m] Residues 470-478.

The structures of the small domain and the invariant part of the large domain are conserved among sugar kinases and some phosphortransferases, whereas the fold of the variable subdomain is specific to hexokinases (32).

Rigid-body conformational changes between N- and C-halves of hexokinase I— Root-mean-squared deviations between superimposed N- and C-halves of G6Pd and G6Pm are 0.45 and 0.60 Å, respectively. (The loop 98-104, poorly ordered in G6Pd, was omitted from the superposition). The root-mean-squared deviation between C_α atoms of polypeptide

chains from G6Pm and G6Pd is, however, 1.9 Å, suggesting a conformational change, which must be due to differences in the relative orientations/positions of the N- and C-halves.

Using the large domain of the C-halves as a basis for superposition, the N-halves of G6Pm and G6Pd exhibit a relative twist of 13° about an axis roughly parallel to that of the transition helix (residues 450-478), which connects the two halves of hexokinase I (Table 3). As depicted in Fig. 3, the twist of 13° can be resolved into a deformation of the transition helix and rotations of the N- and C-halves around the ends of the helix. The elastic deformation is the unwinding of the transition helix by approximately 10°. The transition helices in G6Pm and G6Pd are bent to almost the same extent (24±2° between helical ends, Fig. 3 and Table 3).

Again using the large domain of the C-half as a basis for superposition, the N-halves of G6Pm and P_id exhibit a relative rotation of 26°, which can be resolved as above into a deformation of the transition helix, and rotations of the N- and C-halves about the ends of the transition helix. The transition helix assumes a less bent conformation (not more than a 5° bend) in P_id.

Not all of the rigid-body motions listed in Table 3 are functionally significant. Indeed, rotations of the order of 2° and less may result from differences in packing interactions. More problematic are the effects of subunit interactions in G6Pd and P_id, which are absent in G6Pm. The bent transition helix, however, appears in G6Pm and G6Pd despite major differences in subunit and lattice contacts, and could be an intrinsic property of G6P-bound hexokinase I. The unbending of the transition helix in P_id may arise from P_i-ligation of the N-half, the influence of subunit contacts of the dimer, and/or the influence of a C-half

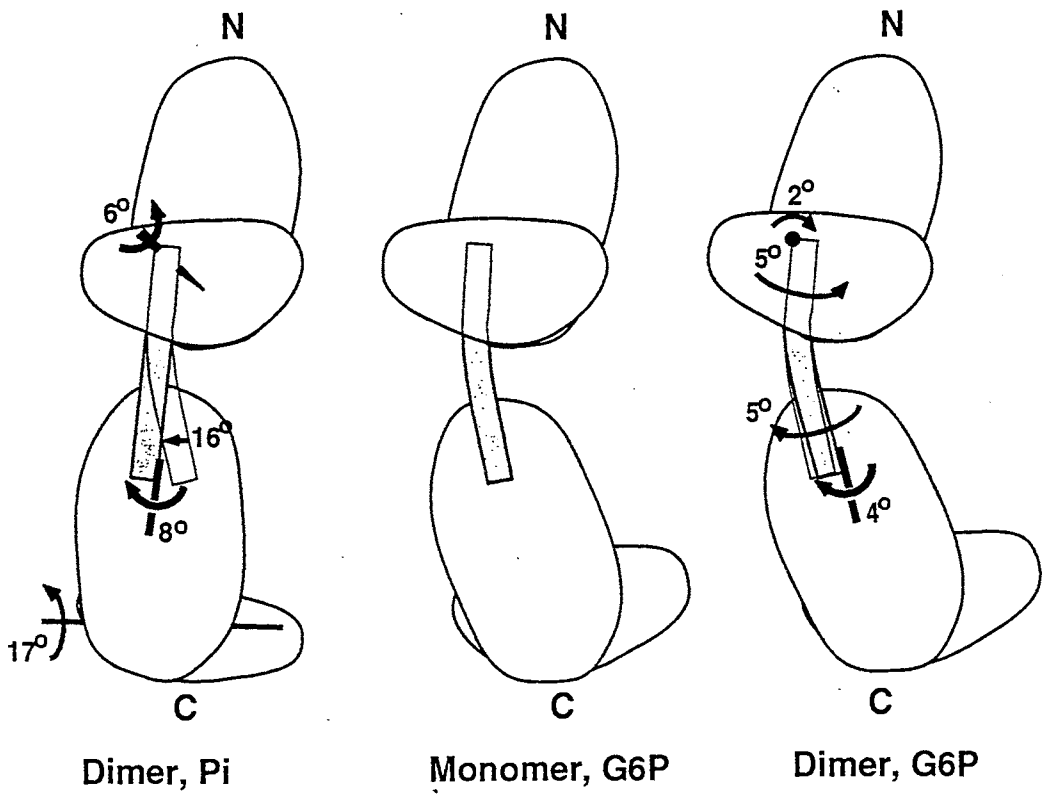

Figure 3. Schematic of conformational differences between subunits from the G6Pm, G6Pd and P_id crystal forms. The subunit in G6Pm (labeled as monomer, G6P) undergoes rigid-body rotations of its N- and C-halves and elastic deformations of its transition helix. The C-half rotates about axes approximately parallel to the C-terminal end of the transition helix, whereas the N-half rotates about axes approximately perpendicular to and positioned at the N-terminus of the transition helix. The transition helix unwinds by 10° in G6Pd relative to G6Pm and straightens by 16° in P_id relative to G6Pm. In addition the small domain of the C-half rotates by approximately 17° in P_id about an axis that lies between the small and large domains of the C-half.

in an open conformation. The functional consequence of a straight transition helix is conjecture, although clearly such a conformational change could influence non-covalent interactions, which couple the N- and C-halves. The rotation of the C-half about the C-terminus of the transition helix is qualitatively similar in P_id and G6Pd. Evidently, the C-half of hexokinase I can rotate rather easily about this point, and dimerization may significantly influence the extent of that rotation. The rotation of the N-half about the N-terminus of the transition helix appears, however, only in P_id. The observed 6° rotation may not be a consequence of dimer formation, but rather to differences in the state of ligation of the N-half, as discussed below.

Conformational differences in P_i- and G6P-ligated N-halves— If G6P and P_i are allosteric antagonists, then N-halves ligated by G6P/Glc and P_i/Glc must differ in conformation. Such differences were not obvious in a comparison of N-halves from G6Pd and P_id (6), but with added information from G6Pm (which binds G6P/Glc), we observe reproducible differences, that may be relevant to the allosteric regulation of catalysis in hexokinase I. As noted above, the N-half of P_id is rotated approximately 6° relative to the N-halves of G6Pm and G6Pd (Table 3). Loop 447-450, which precedes the transition helix, has a different conformation with much higher B-parameters in P_id, than in G6Pm or G6Pd (average B for main-chain atoms of residues 447-450 in P_id, G6Pd and G6Pm are 83, 46, and 27 $Å^2$, respectively). When P_i displaces G6P in crystals of ADPm the positional and thermal parameters of the loop do not change. Only when hexokinase I is co-crystallized with P_i and Glc from solution, does a new conformation occur for the loop (Fig. 4). Evidently, the conformation of the loop and the position of the transition helix are correlated. Ser449 of loop 447-450 makes a critical hydrogen bond to the 2-hydroxyl group of G6P in G6Pd and

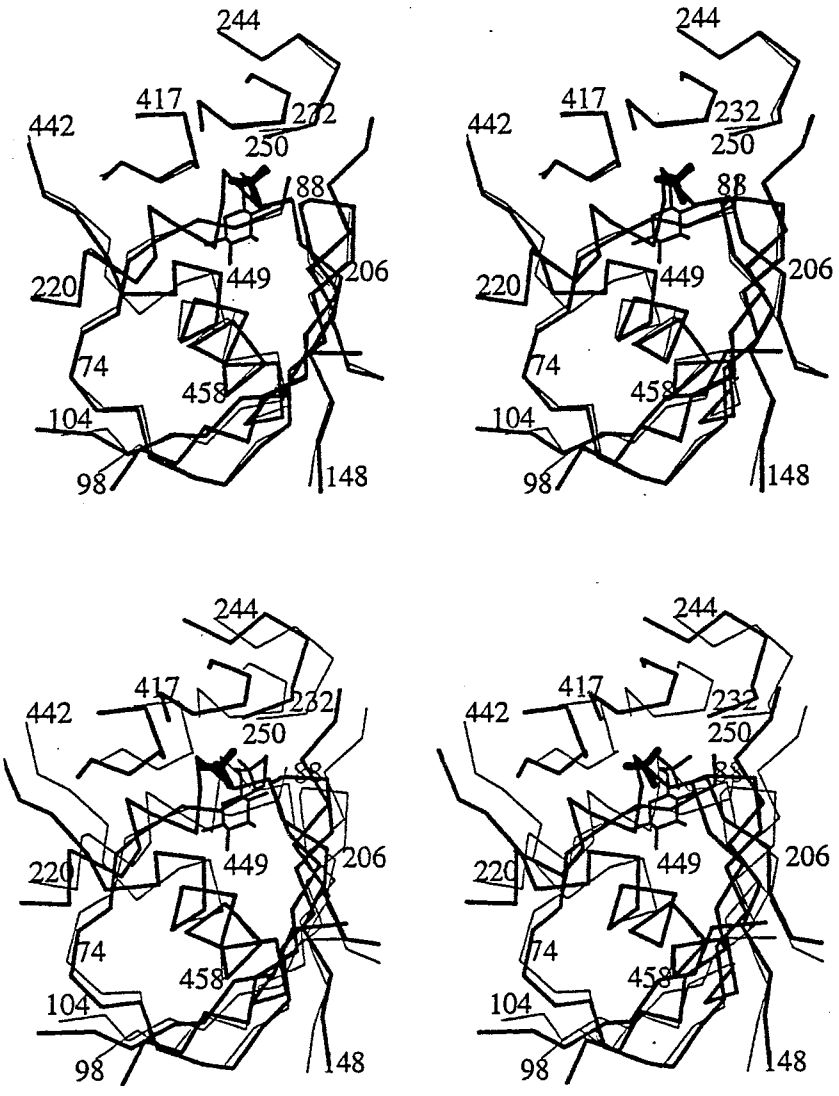

Figure 4. Conformational differences in P_i- and G6P-bound N-halves of hexokinase I. Top: Stereoview of the N-half from P_id (bold lines) superimposed over the N-half of G6Pm, using the entire N-half as the basis for superposition. The superposition reveals a significant difference in conformation in the vicinity of residue 449 (serine). Bottom: Stereoview of the N-half of P_id (bold lines) superimposed over the N-half of G6Pm using the N-terminal half of the transition helix as the basis for superposition. The entire N-half pivots about the N-terminus of the transition helix.

G6Pm. The loss of the hydrogen bonds between Ser449 and G6P, evidently allows the N-half to rock 6° about the transition helix (Fig. 4). The sequence of the N-terminal half of the transition helix is rich in small side-chain amino acids (alanine and glycine), which offer little steric resistance to re-orientations of that helix within the hydrophobic core of the N-half. The rotation of the N-half causes a significant shift in the position of loop 249-252, a structural element, which putatively communicates the state of ligation of the N-half to the C-half. Furthermore, the observed rotation of the N-half in P_id relative to G6Pm may be limited by dimerization. The observed rotations will not have a significant influence on the global conformation of hexokinase I, as is consistent with results from small angle X-ray scattering (26).

Although P_i can directly displace G6P and thereby relieve G6P-inhibition, it is not an activator of catalysis in assays where Glc saturates its binding sites. If the N-terminal domain of hexokinase I is closed by Glc alone, then P_i-bound and P_i-free states of the N-half could be conformationally identical, and hence have the same effect on catalysis at the C-half. Indeed, Glc alone can close yeast hexokinase (33).

Conformational differences in the flexible element— Aleshin *et al.* (1998a) noted previously that the N- and C-terminal halves of G6Pd superimpose on each other well except for residues 320-362 and 768-810. These regions were called flexible subdomains. Residues 768-810 interact between subunits of the dimer and between N- and C-halves within a subunit. In G6Pm and ADPm these interactions are gone. Indeed, the flexible elements in G6Pm and ADPm are free of lattice contacts. Although the average B-parameter of G6Pm is significantly less that that of G6Pd, the thermal parameters for residues 793-812 are 2- to 3-fold higher (Fig. 2). Residues 759-772, 794-808, and 811-817 of G6Pm shift 0.4-1.0 Å and

now have conformations more similar to the corresponding elements of the N-half. This shift is due in part to the rigid body motion of the variable subdomain (see Table 3). Hence, dimerization has a significant influence on the conformation of the flexible element, and in the absence of inter- and intra-molecular contacts, this element becomes mobile. Mobile or flexible elements often participate in mechanisms of signaling and allosteric regulation.

New orientation for the pyranosyl group of G6P— The G6P molecules in G6Pm (at 1.9 Å resolution) and G6Pd (at 2.8 Å resolution) differ by a rotation of their pyranosyl groups by 180° about the covalent bond between atoms C5 and C6. Protein side chains, identified previously in G6Pd, still hydrogen bond to the pyranosyl group, but now with different hydroxyl groups (Table 4). As the 2-hydroxyl group is near the axis of the C5-C6 covalent bond, its position and hydrogen bonds with the protein remain unchanged. One face of the glucosyl moiety packs against the protein, whereas the other is exposed to ordered water molecules. Carbon-1 of the pyranosyl group is in the β-configuration (Fig. 4). In G6Pm we observed sharp electron density corresponding to the pyranosyl group, whereas in G6Pd electron density for the pyranosyl group indicated the possibility of alternative conformations (5). The new orientation for the pyranosyl group places the 1-OH group near the surface at the open end of the G6P pocket. Hence, the inhibitor, glucose 1,6-bisphosphate, would bind without steric interference from the protein. Furthermore, the new conformation for G6P also provides an adequate fit to the electron density in G6Pd. The G6P conformation in G6Pd is probably incorrect; the current deposition of G6Pd (accession identifier, 1HKB) has corrected this error. The high-resolution data from the G6Pm structure confirms the assignment of the α-configuration to C-1 of bound Glc molecules.

Table 4

Selected interactions between ligands and mutant hexokinases in G6Pm and ADPm.

Ligand Atom	Protein contact	Distance (Å)
G6P (C-half/N-half)[a]:		
O1	OD2 Asp 861 / Asp 413	2.32 / 2.52
	OD1 Asp 861 / Asp 413	3.12 / 3.17
O2	N Ser 897 / Ser 449	2.89 / 2.98
	OD1 Asp 532 / Asp 84	2.87 / 2.59
O3	OG Ser 897 / Ser 449	2.77 / 2.77
	OD2 Asp 532 / Asp 84	2.67 / 2.69
	OD1 Asp 532 / Asp 84	3.24 / 3.21
O4	OD1 Asp 651 / Asp 209	2.71 / 2.65
6-Phosphoryl	OG Thr 680 / Thr 232	2.67 / 2.65
	N Thr 680 / Thr 232	2.81 / 2.79
	OG Thr 863 / Ser 415	2.51 / 2.73
	N Thr 863 / Ser 415	3.09 / 3.07
	OG Thr 536 / Ser 88	2.52 / 2.68
	N Thr 536 / Ser 88	2.81 / 2.80
ADP (N-half)[a]:		
N6	O Leu 31	3.28
	OD1 Asn 384	3.25
N1-Wat 12	N Leu 31	2.88
	OD1 Asn 384	3.16
	O Met 29	2.76
O2'	NH Arg 30	3.13
α-Phosphoryl	NH1 Arg 425	2.79
	NE Arg 426	3.09
β-Phosphoryl	NH2 Arg 425	2.86
	NH2 Arg 426	3.24
	OH Tyr 732[c]	2.95
ADP (C-half)[b]:		
N1	OG Ser 788	2.70
N6	O Lys 785	2.90
O2'	O Gly 747	3.00
O5'	OG1 Thr 863	2.70
	N Thr 863	3.20
α-Phosphoryl	OG1 Thr 680	2.80
	N Thr 680	2.60
	N Ala 536[d]	2.70
β-Phosphoryl	N Asn 537	2.90
	N Ala 536[d]	2.90
	ND2 Asn 537	3.10
	OG1 Thr 863	3.30

Table 4
(continued)

[a] Distances are from the structure, shown in column 1 of Table 2. [b] Distances are from the structure, shown in column 4 of Table 2. [c] The lattice contact. [d] Thr 536 in wild type hexokinase.

ADP binding site of the N-half— ADP binds to the N-half at a site well removed from the G6P, P_i and Glc binding pockets (Figs 1 & 5). The ADP molecule bound at the N-half is well-ordered (average thermal parameter of 34 $Å^2$) and even after washing G6Pm crystals extensively in buffers free of ADP, electron density remains at this site. The base moiety of ADP is stacked between the side-chains of Phe380 and Arg30. The 6-amino group and the endocyclic N-1 atom hydrogen bond with the protein directly or through a bridging water molecule (Fig. 5 and Table 4). Arg30 hydrogen bonds with the 2'-hydroxyl group, and His27 either hydrogen bonds with the 3'-hydroxyl group or Asp23, depending on the orientation of its side chain. That latter interaction may allow ADP to exert a direct influence on the orientation of the N-terminal helix, which is involved putatively in the association of hexokinase I with mitochondrial porin (34-39). Arg425 and Arg426 bind to the pyrophosphoryl group of ADP. Magnesium cations, although present in the crystallization buffer, are not associated with the ADP molecule. An additional hydrogen bond to the β–phosphoryl group of ADP comes from a lattice contact (Table 4), which may explain the absolute requirement for ADP in the growth of the G6Pm crystal form. The ADP site at the N-half of hexokinase I is probably functionally significant and not an artifact of lattice contacts in G6Pm crystals. 8-Azido-ATP labels rat hexokinase I somewhere within the first 100 residues (40), suggesting the presence of this ADP binding site on hexokinase I in solution. (Note in Fig. 5 the proximity to ADP of several residues

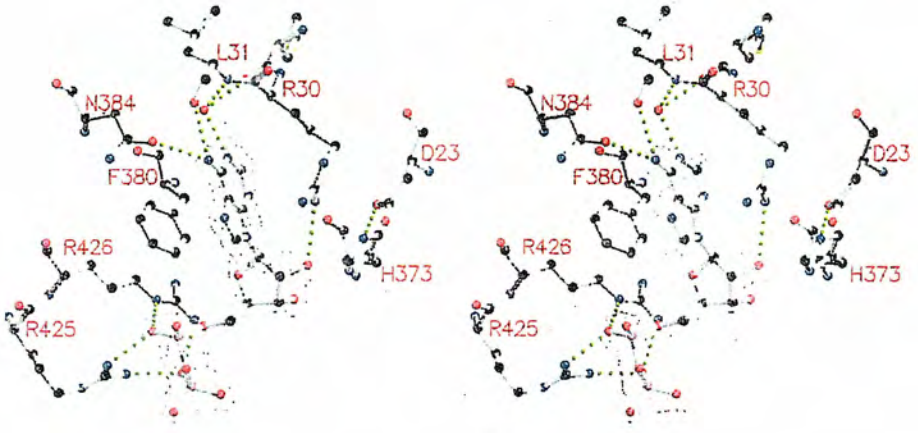

Figure 5. ADP binding site near the N-terminus of hexokinase I. The polypeptide chain and the ADP molecule are represented by ball-and-stick models, with carbon atoms in black, oxygen in red and nitrogen in blue. Electron density from an omit map is at a contour level of 1.4 σ and hydrogen bonds are indicated by dashed green lines.

with sequence numbers below 100). An ADP (or related) molecule bound to this site could mediate association of hexokinase I with the mitochondrial membrane. Alternatively, the ADP site at the N-half could be a "weigh-station" in the transport of adenine nucleotides to and from the mitochondrial matrix. The direct transport of adenine nucleotides to and from membrane-bound hexokinase I has been suggested by several investigations (41-43). The ADP-binding site is not blocked by dimer formation. Hexokinase I putatively binds to mitochondria as an oligomer of uncertain composition (7,37-39,44). Homodimers are the only well-characterized oligomers of hexokinase I.

ADP binding site of the C-half— The α–phosphoryl group of ADP occupies the same site and has the same orientation as the 6-phosphoryl group of G6P. Hence the binding of G6P and adenine nucleotides to the C-half are mutually exclusive phenomena, consistent with kinetics investigations (14). The base moiety of ADP is located between helicies α9 (residues 783-791) and α11' (residues 862-867). [Elements of secondary structure are named in Aleshin *et al.*, (1998a)]. In the G6P-bound C-half the side chain of Thr784 blocks the adenine pocket, but moves to a new position in the presence of bound ADP. The 6-amino group and the N-1 atom of ADP hydrogen bond with backbone carbonyl 785 and the side chain of Ser788, respectively (Fig. 6). The 2'-hydroxyl group hydrogen bonds to backbone carbonyl 747. The side chain of Thr784 is poorly ordered, but one of its staggered conformers could hydrogen bond to the 2'-hydroxyl as well. The α–phosphoryl group makes the same hydrogen bonds as the 6-phosphoryl group of G6P, except for the loss of one interaction due to the mutation at position 536.

The conformational change in Thr784, which opens the adenine pocket, perturbs the first turn of the helix α9 (residues 783-791). Difference electron density maps based on

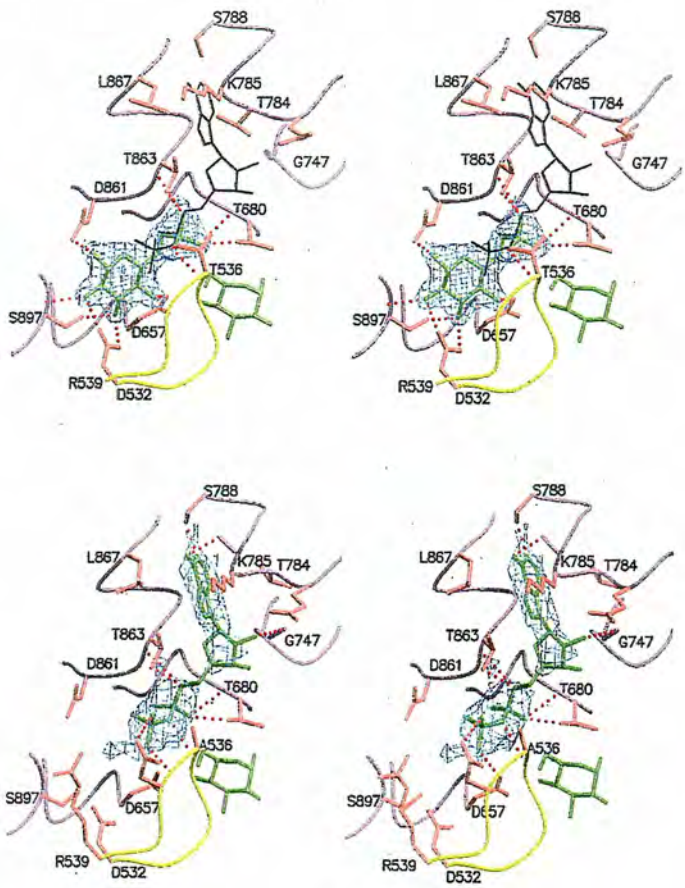

Figure 6. Ligation of the C-half in G6Pm and ADPm. Top: The G6P/Glc-bound C-half of G6Pm at the active site, with G6P and Glc drawn with green lines, selected side chains in orange, elements of the small domain in yellow, and segments of the large subdomain in purple. Donor-acceptor interactions between G6P and the protein are designated by dotted red lines. The electron density (colored blue) covering the G6P molecule is from an omit map, contoured at 1σ. The ADP molecule from ADPm is shown in black to illustrate the overlap of the 6-phosphoryl of G6P with the α-phosphoryl of ADP. Bottom: The ADP/Glc-bound C-half of ADPm at the active site with ADP and Glc drawn with green lines. Other colors take on the same meaning as above. Donor-acceptor interactions between ADP and the protein are designated by dotted red lines. The electron density covering the ADP and G6P molecules is from an omit map, contoured at 1σ.

G6Pm and ADPm indicate small movements in the loop 776-783. More significantly, however, is a conformational change 15 Å away from the adenine pocket in the region of residues 792-797 (Fig. 7). Omit maps of two independent structures of ADPm have consistent, but diffuse electron density in this region (Fig. 8). Hence, the model here is subject to significant uncertainty, as indicated by high thermal parameters. Yet residues 792-797 have significantly different conformations, which carry over to helix α10 (residues 797-807) and loop 808-811 (Fig. 7). Evidently, the movement of Thr784 in response to ADP-ligation displaces residues 776-783 which are in contact with the C-terminal end of the helix α10 (residues 797-807). Hence, the conformational change in residues 792-797 and 797-811 arise putatively from the perturbation of the C-terminal end of helix α10. The structural elements undergoing the largest conformational changes in the C-half, are also involved in the contact interface between N- and C-halves of hexokinase I dimers. Specific mutations in these elements profoundly alter the kinetic properties of hexokinase (45).

Relationships of ADPm to ligand complexes of glycerol kinase— ADP binds to the C-half of hexokinase I as predicted by modeling (5,46,47). The ADP complex of glycerol kinase (48) provided essential information for that modeling effort, and in fact, the active sites of glycerol kinase and hexokinase have significant similarities (Fig. 9). The base of ADP in each enzyme occupies a cleft between two helices, and there are comparable hydrogen bonds with the base, ribose and α-phosphate moieties. The 6-hydroxyl group of glucose in hexokinase corresponds spatially to the 3-hydroxyl group of glycerol in glycerol kinase. The ADP molecules have nearly the same conformation, aside from the location of their β-phosphoryl groups (to be discussed below).

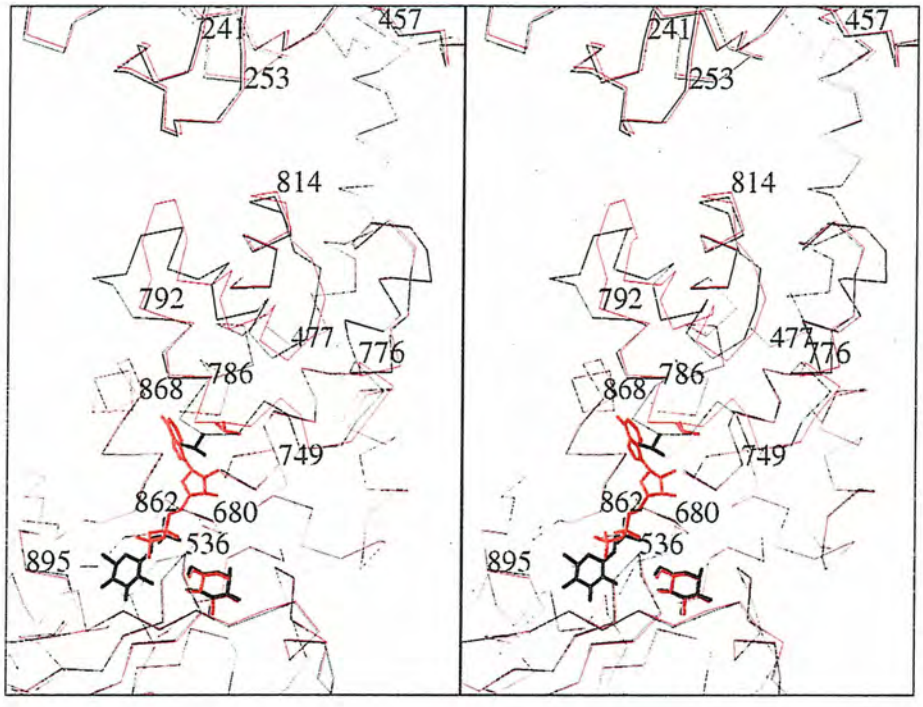

Figure 7. Conformational change in the flexible element induces by ADP displacement of G6P. The C_α trace of ADPm (bold line) and G6Pm diverge in the flexible element (residues 792—813). Two conformations of Thr784 are shown explicitly. The contact interface between halves of the hexokinase I subunit involve interactions between the flexible element and loop 241—253 of the N-half.

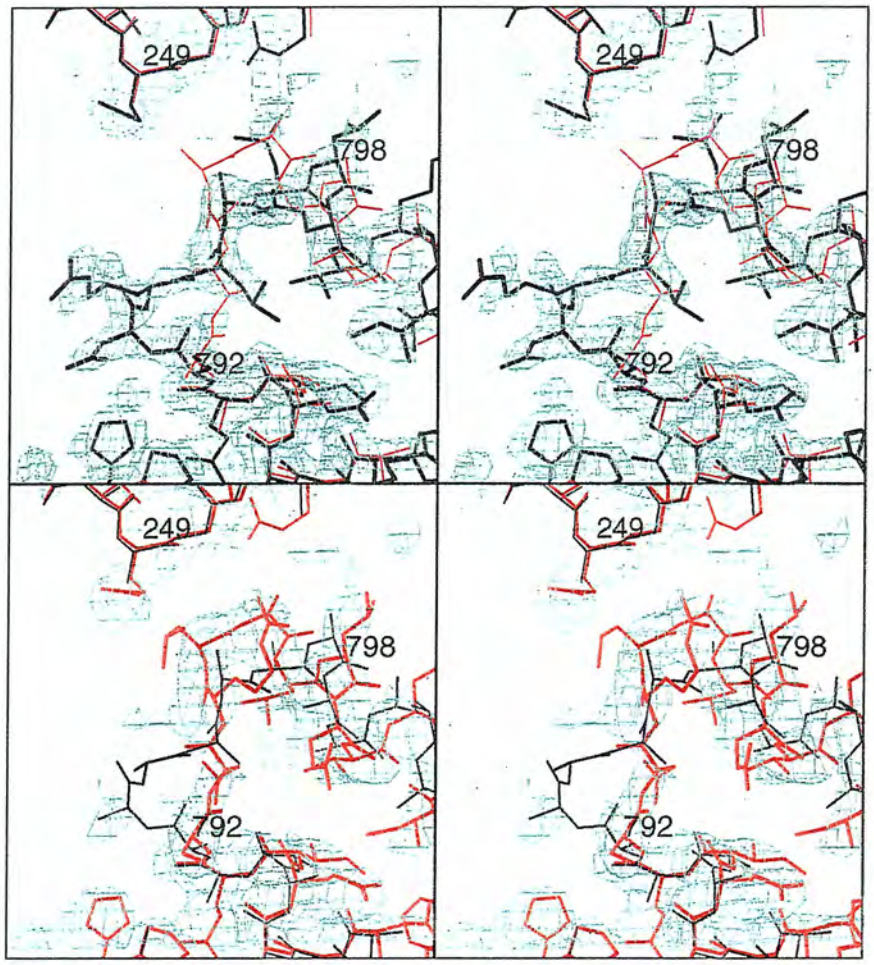

Figure 8. Electron density and refined models for G6Pm and ADPm in the region of the flexible element. Top: G6Pm model in black with electron density from an omit map contoured at 1σ. The backbone for ADPm is in red. Bottom: ADPm model in red with electron density from an omit map contoured at 1σ. The backbone for G6Pm is in black.

Figure 9. Comparison of ADPm to the ADP-complex of glycerol kinase. Left: ADPm with portions of the large domain in purple and the small domain in green. Donor-acceptor interactions are indicated by dashed lines in red. The β-phosphoryl group of ADP is not productively bound due to the presence of loop 532—539. Note that loop 532—539 in the conformation observed for the open C-half (yellow) allows productive binding of the β- and γ-phosphoryl groups of ATP with Mg^{2+} (black lines), but Arg539 and Asp532 are still too far to interact directly the nucleotide. Right: Comparable region of the ADP/glycerol phosphate complex of glycerol kinase, showing hydrogen bonds as dashed red lines.

Irrespective of the similarities noted above, several perhaps significant differences in the ADP complexes of hexokinase I and glycerol kinase are evident. The loops corresponding to residues 533-539 of hexokinase I have similar conformations in the ADP complex of glycerol kinase and in the glucose complex of yeast hexokinase. Yet these same loops differ significantly in conformation from that of hexokinase I (Fig. 9). The conformation of loop 533-539 in hexokinase I is predetermined by the binding of G6P in the growth of G6Pm crystals, and for unknown reasons, does not relax when G6P is washed away from the crystal (49). With loop 533-539 in its G6P-ligated conformation, the β-phosphoryl group of ADP is denied access to the locus of hydrogen bonds identified by reference to the ADP complex of glycerol kinase (Fig. 9). Asp532 and Arg539 of hexokinase I, on the basis of the ADP complex of glycerol kinase, should interact with the β-phosphoryl group of ADP. (Clearly, Mg^{2+} should mediate the interaction between Asp532 and the β-phosphoryl group, as depicted in Fig. 9). A local conformational change in loop 533-539 of hexokinase I to that observed in the open C-half (Fig. 9) would remove a steric block to the true β-phosphoryl pocket, but Arg539 and Asp532 are still too far from the polyphosphoryl pocket to participate in salt links and metal coordination. The domain of glycerol kinase, which has Arg17 and Asp10 (residues corresponding to Arg539 and Asp532 in hexokinase I) has a different relative orientation, than the corresponding domain of hexokinase I (Fig. 9). In order to bring Arg539 and Asp532 into position, an additional domain movement in hexokinase I may be necessary. Hence, the productive ATP/Glc complex of hexokinase I may provide yet another rigid-body relationship between its small and large domains, distinct from the open conformation and the G6P/Glc-closed conformation. The complete removal of G6P and its replacement with ADP gradually

destroys the diffracting power of crystals (Table 2), which is a phenomenon consistent with global conformational differences between C-halves ligated by ATP/Glc and G6P/Glc.

Allosteric mechanism of hexokinase I— In order for an allosteric mechanism to exist, the effector must in some manner selectively stabilize one of at least two different conformational states. The series of structures presented here identifies a specific region of the C-half (flexible element), which in this decoupled system is mobile and exists in at least two different conformations. Only one of the two conformations allows ADP binding to the C-half. In response to ADP binding this same flexible element undergoes a conformational change that would directly alter the contact interface between N- and C-halves of hexokinase I. Hence, if the G6P-bound N-half destabilizes the ATP-bound conformation of the flexible element, one has a basis for allosteric inhibition of catalysis.

P_i-relief of G6P inhibition clearly entails the displacement of G6P from the N-half. P_i in the presence of saturating Glc, however, is not an activator of hexokinase I. If the P_i/Glc-bound N-half is decoupled from the C-half, then no P_i activation is possible, but how then does P_i prevent G6P from directly inhibiting the C-half, as is clearly possible on the basis of recent work by Liu *et al.* (1999). The P_i/Glc-bound N-half must remain coupled to the C-half, but it can stabilize the ATP-bound C-half no more effectively than the Glc-bound N-half. Hence, the P_i/Glc-bound and Glc-bound conformations of the N-half must be nearly identical. As the Pi/Glc-bound N-half is in the closed conformation we suggest that Glc alone will stabilize a closed N-half. Indeed, we have noted previously that the N-half is incapable of forming an interdomain salt-link that putatively stabilizes the C-half in an open conformation (6). Glc, even in the presence of P_i, does not close the C-half in co-

crystallization experiments, as is consistent with a kinetic mechanism, which requires the random addition of substrates to the active site.

As the coupling interface of hexokinase I may have only a single hydrogen bond, an appreciable fraction of the enzyme may exist as an uncoupled monomer. An uncoupled form of the enzyme is present in the crystal structures reported here. In the uncoupled monomer, each half behaves independently. G6P/Glc binds to the N-half and to the C-half, but the binding of G6P/Glc (and presumably P_i/Glc) to the N-half is kinetically silent. Evidently, the adenine nucleotide can stabilize its base-binding pocket without the benefit of coupling interactions, which is consistent with the observation of appreciable activity for the truncated C-terminal half.

The status of hexokinase I on the mitochondrial membrane is uncertain, but recent studies indicate hexokinase I in its membrane-bound state is an oligomer (37-39). Membrane-associated hexokinase I and hexokinase I monomers in solution, however, exhibit similar kinetic phenomena (43,50,51). Hence, a better understanding of the conformational states of the hexokinase I monomer, should help develop our understanding of structure-function relationships of the membrane-associated enzyme.

Experimental

Materials—A full-length cDNA of human brain hexokinase, cloned into an expression vector pET-11a (from Novagen) to produce pET-11a-HKI, was available from previous studies (18,26). The Transformer site-directed mutagenesis kit is from Clonetech Laboratories, Inc. T4 polynucleotide kinase and all restriction enzymes are from Promega. Bio-gel hydroxyapatite resin is from Bio-Rad. Toyopearl DEAE-650M is from Tosohaas.

The Iowa State University Nucleic Acid Facility performed oligonucleotide synthesis and DNA sequencing. *E. coli* strain ZSC13(DE3), which does not contain endogenous hexokinase, was a gift from the Genetic Stock Center, Yale University. ATP, ADP, NADP, 1,5-Anhydro-D-sorbitol, deoxyribonuclease I (Dnase I), leupeptin, phenylmethylsulfonyl fluoride (PMSF), ampicillin and polyethylene glycol 8000 (PEG 8000) are from Sigma. Glucose-6-phosphate dehydrogenase came from Boehinger Manheim. Isopropyl-1-thio-β-D-galactopyronoside (IPTG) is from BioWorld.

Directed mutation, expression, purification and kinetics— The triple mutant of hexokinase I (Glu280→Ala, Arg283→Ala, Gly284→Tyr) was constructed and kinetically characterized in a previous study (26). The quadruple mutant was constructed by directed mutation of the triple mutant, according to the protocols of the Clontech Transformer site-directed mutagenesis kit. The mutant plasmid was selected from wild-type plasmids by switching a unique *Nru*I restriction site on the pET-11 vector to another unique *Xho*I site for the single point mutation. The primer for mutation Thr536→Ala is 5'-GATCTTGGAGGA**GCA**AATTTCCGTG-3', where the modified codon is in bold typeface and underlined. The oligonucleotide primers used for the selection of the mutant plasmid from the wild-type plasmid are 5'-CAGCCTCGC**CTCGAG**AACGCCAGCAAG-3', for the conversion from the NruI site to the XhoI site, and 5'-CCTCGC**GTCGCG**AACGCCAGCAAG-3', for the conversion from the XhoI site back to the NruI site. Mutations were confirmed by sequencing the entire cDNA insert, coding for hexokinase I.

E. coli strain ZSC13, transformed with mutant pET-11a-HKI, were grown in LB medium at 37° C to an OD_{600} of 0.8, whereupon the temperature was reduced to 22° C and

IPTG added to a final concentration of 0.4 mM. Sixteen to 24 hours after induction, the cells were harvested and then re-suspended in 25 mM KP_i (pH 7.5), 2 mM glucose, 1 mM EDTA, 0.4 mM 2-mercaptoethanol, 1 mM PMSF, and 3000 units of Dnase I at a temperature of 4° C. The cells were broken using a French press and centrifuged, after which the supernatant was passed through a DEAE column, using a KP_i-buffered (pH 7.5), KCl gradient from 0 to 0.5 M. The fractions containing HKI were concentrated and then passed though a hydroxyapatite column using a KP_i-buffered (pH 7.5), KCl gradient from 20—500 mM. Pooled fractions of mutant hexokinase I were further purified by DEAE-HPLC, as described elsewhere (5).

Hexokinase activity was determined by a coupled spectrometric assay, using G6P-dehydrogenase (52). 1,5-Anhydroglucitol-6-phosphate (1,5-AnG6P) is a surrogate for G6P in kinetic studies of G6P inhibition. (The coupling enzyme degrades G6P but not 1,5-AnG6P). 1,5-AnG6P was prepared as described elsewhere (53). Commercial glucose-6-phosphate dehydrogenase comes as an ammonium sulfate precipitate. Sulfate anion, which mimics the effect of P_i in the relief of G6P inhibition (16), was removed by dialysis. Hexokinase concentrations were determined by Bradford assays using bovine serum albumin as a standard (54). Initial rate data were analyzed by using a computer program written in MINITAB with an α-value of 2.0 (55). In experiments with 1,5-anhydroglucitol 6-phosphate the kinetic data were fit to a model for nonlinear competitive inhibition with respect to ATP, in which two molecules of inhibitor interact sequentially with hexokinase I (18).

Crystal preparation— Crystals of the triple and quadruple mutants were grown by the hanging drop method. Two protocols produced the same crystal form. In the first, hexokinase I mutants were transferred from a storage buffer (30 mM KP_i, pH 7.5, 1mM Glc,

1mM β-mercaptoethanol) to a buffer consisting of 25 mM ADP, pH 7.5, and 1 mM Glc. Equal volumes (2.5 μL) of the protein solution (20 mg/ml of mutant enzyme in the buffer above) and a precipitant solution [14-18% (w/v) PEG 8000, 100mM 2-*N*-morpholinoethanesulfonic acid (MES), pH 5.8-6.5, 200 mM sodium acetate, 20 mM ADP, 2 mM $Al(NO_3)_3$, 10 mM NaF, and 30 mM magnesium acetate] were mixed. The drops were equilibrated against 0.7 ml of the precipitant solution. One crystal (dimensions, 0.15 x 0.15 x 0.05 mm) appeared per droplet. Although G6P was not added the crystalline enzyme had two G6P molecules bound with high occupancies. Evidently, G6P was produced by hexokinase from glucose and an ATP contaminant in the ADP. The amount of ATP impurity (0.16%) was determined by a yeast hexokinase, G6P-dehydrogenase coupled spectrometric assay (52), using excess of glucose and NADP. The importance of G6P for the growth of this crystal form follows not only from the high ligand occupancy, but also from the failure to grow crystals with purified ADP. Contaminating ATP was removed from ADP by the coupled assay system above. A solution containing 250 mM of impure ADP, 3 units each of yeast hexokinase and G6P-dehydrogenase, 10 mM magnesium acetate, 1 mM NADP, and 1 mM Glc was incubated for 2 hours at 24° C, and then filtered through a pressure concentrator with a molecular weight cut-off of 14 kDa. The "purified ADP" was stored frozen.

In the second crystallization protocol, the protein was dialyzed against 1 mM Glc and 20 mM G6P, pH 7.5, and then concentrated to 20 mg/ml. Equal volumes (2.5 μL) of the protein solution and a precipitant solution (14-18% PEG 8000, 100 mM MES, pH 5.8-6.5, 150-250 mM sodium acetate and 20 mM ADP) were mixed. The high concentration of G6P, used in the second protocol, provided crystals of bigger size (0.4 x 0.3 x 0.2 mm).

Two crystals of the triple mutant, reported in columns 1 & 2 of Table 2, were grown by the first protocol (without addition of G6P). The data of Table 2, column 1, comes from a crystal which was soaked for 12 hours at 22° C in a solution containing 20% PEG 8000, 50 mM MES, pH 6.5, 100 mM sodium acetate, 30 mM ADP, 30 mM magnesium acetate, 1 mM $Al(NO_3)_3$, 20 mM NaF, and 1mM Glc. Table 2, column 2, presents data from a crystal which was soaked for 10 hours in a solution containing 20% PEG, 50 mM MES, pH 6.5, 100 mM sodium acetate, 0.6 mM G6P, and 1mM Glc. The solutions were refreshed every 3 hours throughout the duration of the soaks.

The crystals of the quadruple mutant grew only by the second protocol. G6P was removed from the crystals by soaking in G6P-free solutions. Crystals were transferred to solutions containing 20% PEG 8000, 50 mM MES, pH 6.5, 50 mM sodium acetate, 1 mM DTT, 40 mM magnesium acetate, and 100 mM of unpurified ADP. One crystal then was soaked for 1.5 hours in the solution above prepared with purified ADP, 1 unit of G6P-dehydrogenase, and NADP (Table 2, column 3). The second crystal was soaked for 5 hours in a similar solution (Table 2, column 4).

Glycerol was added to soaking solutions to a final concentration of 25% (v/v) prior to flash-freezing crystals in liquid nitrogen.

Data collection— X-ray diffraction data were collected from the crystal of Table 2, column 1, on the beamline of Dr. Bartunik at Deutsches Elektronen Synchrotron (DESY), using a MAR CCD detector. The data from crystals of Table 2, columns 2-4, were collected at BioCARS, Sector 14, at the Advanced Photon Source (APS), Argonne National Laboratory. Data were processed with programs Denzo/Scalepack (56), DPS/Mosfilm (57) and Scala (58).

Structure determination and refinement— The crystal structure of the triple mutant (Table 2, column 1) was determined by molecular replacement, using the subunit from G6Pd (PDB entry 1HKB). The N- and C-halves of hexokinase I were positioned independently in the unit cell. The program AmoRe (59) was used in calculation of rotation and translation functions, based on data to 4 Å, and then used again in the rigid body refinement of the N- and C-halves, against data to 3 Å resolution (final rigid-body R-factor of 0.37).

Model building and refinement— Refinement of the triple mutant structure (Table 2, column 1) used ARP (60), Refmac (61), programs from the CCP4 package, and parameters from Engh & Huber (62). The refinement was monitored by the decline in R_{free}, based on 5% of the data randomly excluded from the refinement process. The protein molecule was split into its 4 domains, which were refined as rigid bodies. The program ARP, combined with Protin, Refmac, and Sigmaa, was used for restrained refinement and the calculation of electron density maps. Adjustments to the model were accomplished with XtalView (63) and O (64). The first 80% of water molecules were added automatically (3σ cut off applied to a F_{obs}-F_{calc} Fourier map) and refined with the solvent building routine of ARP. Restrained refinement by Refmac with anisotropic scaling and minimization by the maximum likelihood method were used. The final 20% of water molecules were added manually and ambiguous areas were rebuilt using omit electron density maps produced with Refmac and Sigmaa.

The structure presented in Table 2, column 2, employed the refined structure from Table 2, column 1, but with ligands and water molecules omitted. After independently reconstructing the solvent, the location of water molecules was verified by their presence in both structures. The structures presented in Table 2, columns 3-4, were of modest resolution, making the use of ARP impractical. The models reflect the restrained refinement of

individual parameters, but such refinement did not improve R_{free}. The conformation of ligands and protein residues were verified by the comparison of electron density maps from two crystals, prepared independently by the same protocol. Generally, water molecules were fit to peaks of difference density maps higher than 3σ, only if the corresponding positions were occupied in the high-resolution structures of the triple mutant. Exceptions to this rule were made in areas, which had undergone a conformational change.

The analysis of root mean square deviations in the positions of Ca atoms of different models employed the program LSQKAB of the CCP4 package. This program was also used to superimpose the glycerol kinase structure (48) onto the hexokinase I structures, and to determine the differences in the orientation of individual domains in hexokinase I structures. The rotations about polar axes, listed in Table 3, were extracted from rotation matrices determined by superposition. The bend of the transition helix was determined by inspection, using graphics programs.

Acknowledgement

This research was supported in part by Grant NS 10546 from the National Institutes of Health, United States Public Health Service, Grant MCB-9603595 from the National Science Foundation, and Grant 95-37500-1926 from the United States Department of Agriculture.

References

1. Lowry, O.H. & Passonneau, J.V. (1964) *J. Biol. Chem.* **239**, 31-42.

2. Katzen, H. M. & Schimke, R. T. (1965) *Proc. Natl. Acad. Sci. USA* **54**, 1218-1225.

3. Schwab, D. A. & Wilson, J. E. (1989) *Proc. Natl. Acad. Sci. USA* **86**, 2563-2567.

4. Wilson, J. E. (1995) *Rev. Physiol. Biochem. Pharmacol.* **126**, 65-198.

5. Aleshin, A. E., Zeng, C., Bourenkov, G. P., Bartunik, H. D., Fromm, H. J. & Honzatko, R. B. (1998a) *Structure* **6**, 39-50.

6. Aleshin, A. E., Zeng, C., Bartunik, H. D., Fromm, H. J. & Honzatko, R. B. (1998b) *J. Mol. Biol.* **282**, 345-357.

7. Aleshin, A. E., Fromm, H. J. & Honzatko, R. B. (1998c) *FEBS Lett.* **434**, 42-46.

8. Mulichak, A. M., Wilson, J. E., Padmanabhan, K, & Garavito R. M. (1998) *Nature Struct. Biol.* **5**, 555-560.

9. Easterby, J. S. & O'Brien, M. J. (1973) *Eur. J. Biochem.* **38**, 201-211.

10. Holroyde, M. J. & Trayer, I. P. (1976) *FEBS Lett.* **62**, 215-219.

11. Ureta, T. (1982) *Comp. Biochem. Physiol.* **71B**, 549-555.

12. Manning, T. A. & Wilson, J. E. (1984) *Biochem. Biophys. Res. Commun.* **118**, 90-96.

13. Ureta, T. (1975) in *Isozymes III* (C.L.Markert, Ed.) pp. 575-601, Academic Press, Inc., New York.

14. Ellison, W. R., Lueck, J. D. & Fromm, H. J. (1975) *J. Biol. Chem.* **250**, 1864-1841.

15. Fromm, H.J. (1981) in *The Regulation of Carbohydrate Formation and Utilization in Mammals* (C. M. Veneziale ed.), pp. 45-68, University Park Press, Baltimore.

16. White, T. K. & Wilson, J. E. (1989) *Arch. Biochem. Biophys.* **274**, 375-393.

17. Arora, K. K., Filburn, C. R. & Pedersen, P. L. (1993) *J. Biol. Chem.* **266**, 5359-5362.

18. Fang, T. -Y., Alechina, O., Aleshin, A. E., Fromm, H. J. & Honzatko, R. B. (1998) *J. Biol. Chem.* **273**, 19548-19553.

19. White, T. K. & Wilson, J. E. (1987) *Arch. Biochem. Biophys.* **259**, 402-411.

20. Liu, X., Kim, C. S., Kurbanov, F. T., Honzatko, R. B. & Fromm, H. J. (1999) *J. Biol. Chem.*, submitted.

21. Arora, K. K., Filburn, C. R. & Pedersen, P. L. (1991) *J. Biol. Chem.* **266**, 5359-5362.

22. Magnani, M., Bianchi, M., Casabianca, A., Stocchi, V., Daniele, A., Altruda, F., Ferrone, M. & Silengo, L. (1992) *Biochem J.* **285**, 193-199.

23. Zeng, C. & Fromm, H. J. (1995) *J. Biol. Chem.* **270**, 10509-10513.

24. Mehta, A., Jarori, G. K. & Kenkare, U. W. (1988) *J. Biol. Chem.* **263**, 15492-15497.

25. Wilson, J. E. (1973) *Arch. Biochem. Biophys.* **159**, 543-549.

26. Aleshin, A. E., Malfois, M., Liu, X., Kim, C. S., Fromm, H. J., Honzatko, R. B., Koch, M. H. J. & Svergun, D. I. (1999) *Biochemistry* **38**, 8359-8366.

27. Laskowski, R. A., MacArthur, M. W., Moss, D. S. & Thornton, J. M. (1993) *J. Appl. Crystallog.* **26**, 283-291.

28. Murshudov, G. N. & Dodson, E. L. (1997) *in CCP4 Newsletter on Protein Crystallography No 33* (Winn, M., ed.) pp. 31-39, Daresbury Laboratory, Warrington, UK.

29. Bartunik, H. D., *unpublished.*

30. Kraulis, J. (1991) *J. Appl. Crystallog.* **24**, 946-950.

31. Merritt, E. A. & Murphy, M. E. P. (1994) *Acta Crystallogr.* D**50**, 869-873.

32. Bork, P., Sander, C. & Valencia, A. (1992) *Proc. Natl. Acad. Sci.* USA **89**, 7290-7294.

33. Bennett, W. S., Jr. & Steitz, T. A. (1980) *J. Mol. Biol.* **140**, 211-230.

34. Polakis, P. G. & Wilson, J. E. (1985) *Arch. Biochem. Biophys.* **236**, 328-337.

35. Xie, G. & Wilson, J. E. (1988) *Arch. Biochem. Biophy.* **267,** 803-810.

36. Wicker, U., Bücheler, K., Gellerich, F. N., Wagner, M., Kapischke, M. & Brdiczka, D. (1993) *Bioch. Biophys. Acta* **1142**, 228-239.

37. Beutner, G., Rück, A., Riede, B., Welte, W. & Brdiczka. (1996) *FEBS Lett.* **396**, 189-195.

38. Beutner, G., Rück, A., Riede, B. & Brdiczka (1997) *Biochem. Soc. Trans.* **25**, 151-157.

39. Beutner, G., Rück, A., Riede, B. & Brdiczka. (1998) *Bioch. Biophys. Acta* **1368**, 7-18.

40. Nemat-Gorgani, M. & Wilson, J. E. (1986) *Arch. Biochem. Biophys.* **251**, 97-103.

41. BeltrandelRio, H. & Wilson, J. E. (1992) *Arch Biochem Biophys* **299**, 116-124.

42. Laterveer, F. D., Gellerich, F. N. & Nicolay, K. (1995) *Eur. J. Biochem.* **232**, 569-577.

43. de Cerqueira Cesar, M. & Wilson, J. E. (1998) *Arch. Biochem. Biophys.* **350**, 109-117.

44. Xie, G. & Wilson, J. E. (1990) *Arch. Biochem. Biophys.* **276**, 285-293.

45. Kim, C. S. & Fromm, H. J., *unpublished.*

46. Zeng, C., Aleshin, A. E., Hardie, J. B., Harrison, R. W. & Fromm, H. J. (1996) *Biochemistry* **35**, 13157-13164.

47. Zeng, C., Aleshin, A. E., Guanjin, C., Honzatko, R. B. & Fromm, H. J. (1998) *J. Biol. Chem.* **273**, 700-704.

48. Hurley, J. H., Faber, H. R., Worthylake, D.,Meadow, N. D., Roseman, S., Pettigrew, D. W. & Remington, S. J. (1993) *Science* **259**, 673-677.

49. Aleshin, A. E. & Honzatko, R. B., *unpublished.*

50. Rose, I. A. & Warms, J. V. B. (1967) *J. Biol. Chem.* **242**, 1635-1645.

51. Purich, D. L. & Fromm, H. J. (1971) *J. Biol. Chem.* **246**, 3456-3463.

52. Fromm, H. J. & Zewe, V. (1962) *J. Biol. Chem.* **237**, 1661-1667.

53. Ferrari, R. A., Mandelstam, P. & Crane, R. K. (1959) *Arch. Biochem. Biophys.* **80**, 372-377.

54. Bradford, M. M. (1976) *Anal. Biochem.* **72**, 248-254.

55. Siano, D. B., Zyskind, J. W. & Fromm, H. J. (1975) *Arch. Biochem. Biophys.* **170**, 587-600.

56. Otwinowski, Z. (1993) in *Proceedings of the CCP4 study weekend: data collection and processing*, compiled by: L.Sawyer, N. Isaacs & S. Bailey, SERC Daresbury Laboratory, England, pp. 56-62.

57. Steller, I., Bolotovsky, R. & Rossmann, M.G. (1997) *J. Appl. Crystallog.* **30**, 1036-1040.

58. Collaborative Computational Project, Number 4. (1994) *Acta Crystallog. sect. D*, **50**, 760-763.

59. Navaza, J. (1994) *Acta Crystallog. sect. A*, **50**, 157-163.

60. Lamzin, V.S. & Wilson, K.S. (1993) *Acta Cryst*allog. *sect D*, **49**, 129-149.

61. Murshudov, G.N, Vagin, A.A & Dodson, E.J. (1997) *Acta Crystallog. sect D*, **53**, 240-255.

62. Engh, R. A. & Huber, R. (1991) *Acta Crystallog. sect. A,* **47**, 392-400.

63. McRee, D. E. (1992) *J. Molecular Graphics* **10**, 44-46.

64. Jones T.A, Zou, J.Y., Cowan, S.W. & Kjeldgaard, M. (1991) *Acta Crystallog. sect. A*, **47**, 110-119.

CHAPTER 3. GENERAL CONCLUSIONS

Most publications studying hexokinase I are based on the monomeric form of the enzyme, making the determination of the structure of hexokinase I as a monomer an important step in understanding its mechanism. On the basis of small angle x-ray scattering, hexokinase I, even in its monomeric state, adopts a rod-like conformation. The new structural information also supports previous studies which suggest that the allosteric mechanism of the enzyme functions through interactions between a loop containing residues 249-252 in the N-terminal half and residues 801-813 in the C-terminal half as opposed to interactions between monomeric units of the dimer.

G6P acts as an inhibitor of hexokinase I and P_i relieves this inhibition. Hence there must be a ligand-based conformational difference in the N-terminal half of the enzyme. While no changes were obvious in the previously determined dimeric structures, the structure of the monomer emphasized a small conformational difference, heretofore overlooked, in the vicinity of Ser449. The 2-OH of G6P binds to Ser449, whereas P_i cannot. As a consequence the N-terminal half could rotate 6° and change the contacts at the putative allosteric interface between the N- and C-terminal halves.

Crystals soaked with ADP revealed an unexpected binding site for ADP near the N-terminus, potentially allowing ADP to influence the position of the N-terminal helix, which is thought to participate in binding of hexokinase I to mitochondrial porin. ADP also binds to the C-terminal half of hexokinase I, its binding site overlapping with that of G6P, providing a clear explanation for kinetic competition between ATP and G6P for the active site. Although ADP is bound nonproductively at the active site, it serves as a basis for

modeling the productive association of ATP and implicates Thr784 in the mechanism of allosteric inhibition of catalysis.

Recent kinetic experiments in conjunction with the monomeric structures of hexokinase I have led to a revised theory on the allosteric mechanism of the enzyme. While G6P inhibition was originally believed to occur at the C-terminal half of the enzyme, new information allows for the possibility of inhibition by way of the N-terminal half.

Further work on hexokinase I must be done in order to gain a clear understanding of its catalytic and allosteric mechanisms. A crystal structure which shows ATP bound productively at the active site will be an important advance, but a complete understanding of hexokinase I function requires its structure in the context of the mitochondrial membrane.

APPENDIX. ENTRAPMENT OF 6-THIOPHOSPHORYL-IMP IN THE ACTIVE SITE OF CRYSTALLINE ADENYLOSUCCINATE SYNTHETASE FROM ESCHERICHIA COLI

A paper published in the Journal of Biological Chemistry[1]

Bradley W. Poland, Christina Bruns, Herbert J. Fromm, and Richard B. Honzatko

Abstract

Crystal structures of adenylosuccinate synthetase from *Esherichia coli* complexed with Mg^{2+}, 6-thiophosphoryl-IMP, GDP and hadacidin at 298 and 100 K have been refined to *R*-factors of 0.171 and 0.206 against data to 2.8 and 2.5 Å resolution, respectively. Interactions of GDP, Mg^{2+} and hadacidin are similar to those observed for the same ligands in the complex of IMP, GDP, NO_3^-, Mg^{2+} and hadacidin (1). Although crystals were grown from solutions containing 6-mercapto-IMP and GTP, the electron density at the active site is consistent with 6-thiophosphoryl-IMP and GDP. Asp-13 and Gln-224 probably work in concert to stabilize the 6-thioanion of 6-mercapto-IMP, which in turn is the nucleophile in the displacement of GDP from the γ-phosphate of GTP. Once formed, 6-thiophosphoryl-IMP is stable in the active site of the enzyme under the conditions of the structural investigation. The direct observation of 6-thiophosphoryl-IMP in the active site is consistent with the putative generation of 6-phosphoryl-IMP along the reaction pathway of the

---

[1] Reprinted with permission of *J. Biol.Chem.* 1997, 272 (24) 15200-15205.

synthetase.

Introduction

6-mercaptopurine is used in the treatment of pediatric leukemia and other cancers (2). The drug is transformed enzymatically to 6-mercapto-IMP and then into other derivatives such as 6-thio-GTP, 6-thio-ITP and 6-thiomethyl-IMP. 6-Thio-GTP can be incorporated into DNA, increasing the susceptibility of DNA to damage. 6-Thiomethyl-IMP is a potent inhibitor of phosphoribosylpyrophosphate amidotransferase, suppressing *de novo* purine biosynthesis, and 6-mercapto-IMP is a potent inhibitor of RNA polymerase. Depletion of the adenine nucleotide pool (specifically ATP) by the action of 6-thio-methyl-IMP reduces levels of *S*-adenosyl-L-methionine, which in turn impedes methylation of DNA and RNA. Although mechanisms for the cytotoxic effects of 6-mercapto-IMP are known, the metabolic pathways by which 6-mercapto-IMP is inactivated as a drug are unclear.

Adenylosuccinate synthetase (IMP:L-aspartate ligase (GDP-forming), EC 6.3.4.4) is likely to play a role in the metabolic effects of 6-mercapto-IMP. The synthetase governs the first committed step in the *de novo* biosynthesis of AMP (3), GTP + IMP + L-aspartate $\leftrightarrow$ GDP + P_i + adenylosuccinate. 6-Mercapto-IMP is a competitive inhibitor with respect to IMP (4-6) and likely inhibits the enzyme *in vivo*. The combination of adenylosuccinate synthetase with adenylosuccinate, GDP, and thiophosphate (reverse reaction) leads to the slow generation of 6-mercapto-IMP, GTP, and aspartate (7). However, 6-mercapto-IMP, GTP, and aspartate in the presence of enzyme (forward reaction) gives no detectable level of adenylosuccinate. This apparent violation of microscopic reversibility has been explained by an equilibrium constant that significantly favors GTP, 6-mercapto-IMP, and aspartate over

GDP, adenylosuccinate, and thiophosphate. The interaction of 6-mercapto-IMP with adenylosuccinate synthetase then may contribute to the suppression of *de novo* purine biosynthesis but only if *in vivo* levels of IMP are low relative to those of 6-mercapto-IMP.

We report here refined crystal structures at 298 and 100 K of adenylosuccinate synthetase from *Escherichia coli*, grown in the presence of 6-mercapto-IMP, GTP, Mg^{2+}, and hadacidin. Hadacidin (see Fig. 1), a fermentation product of *Penicillium frequentans* (8), is a competitive inhibitor ($K_i \sim 10^{-6}$ M) with respect to aspartate (5,6); the only known function of hadacidin is the inhibition of adenylosuccinate synthetase (9). In the mechanism proposed for the synthetase by Lieberman (10), the γ-phosphate of GTP is transferred to the 6-oxygen of IMP, whereafter aspartate displaces phosphate from the 6-phosphoryl intermediate to form adenylosuccinate. Although the Lieberman (10) mechanism enjoys substantial support from the literature (11-13), no study has provided direct evidence for the formation of a 6-phosphoryl intermediate. Furthermore, 6-phosphoryl-IMP has never been isolated or synthesized. Regardless of temperature, however, a 6-thiophosphoryl intermediate sits at the IMP binding site in the crystal structures, hence providing the first direct observation of 6-thiophosphoryl-IMP and strong evidence in support of the catalytic mechanism proposed 40 years ago by Lieberman (10).

Materials and Methods

Adenylosuccinate synthetase was prepared as described previously from a genetically engineered strain of *E. coli* (14-15). The protein migrates as a single band on SDS-polyacrylamide gel electrophoresis with an apparent relative molecular weight of 48,000. Hadacidin was provided by Drs. Fred Rudolph and Bruce Cooper (Dept. of Biochemistry and

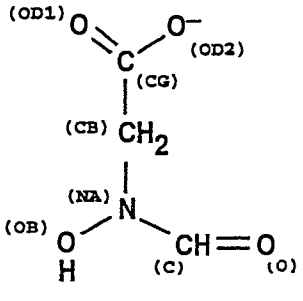

Hadacidin

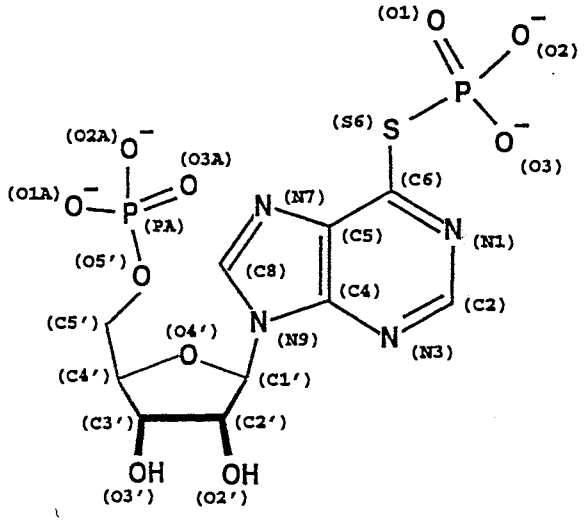

6–Thiophosphoryl–IMP

Figure 1. Diagram of Hadacidin and of 6-thiophosphoryl-IMP, showing labels of atoms.

Cell Biology, Rice University). All other reagents came from Sigma.

Conditions for the growth of the 6-thiophosphoryl-IMP complex were adapted from Poland *et. al.* (1), using the method of hanging drops. Droplets contained 2 μl of enzyme solution (50 mM imidazole, 75 mM succinate, 4 mM GTP, 4 mM 6-mercapto-IMP, 5 mM hadacidin, and 20 mg/ml protein (pH 6.5)) and 2 μl of a crystallization buffer (13% polyethylene glycol 8000 (w/w), 100 mM cacodylic acid/cacodylate (pH 6.5), and 200 mM magnesium acetate). The final pH of the crystallization buffer was 6.5. Wells contained 500 μl of the crystallization buffer. Crystals of approximately 0.5 mm in all dimensions and belonging to the space group $P3_221$ ($a = b = 81.63$ and $c = 159.2$ at 298 K, and $a = b = 80.54$ and $c = 158.2$ and 100 K) grew in about 1 week. The asymmetric unit consists of a monomer.

Data from the 6-thiophosphoryl-IMP complexes were collected on a Siemens area detector at Iowa State University and were reduced by using XENGEN (16). Data sets were 98% complete (see Table I).

Starting phases for the 6-thiophosphoryl-IMP complex were calculated from the IMP/NO_3^- complex (1), omitting coordinates for water molecules, NO_3^-, and IMP. Refinement of the structures involved manual fitting of models to the electron density, using a Silicon Graphics 4D-25 and the program TOM (17), followed by a cycle of refinement using XPLOR (18) on a Silicon Graphics 4D-35. Constants of force and geometry for the protein came from Engh & Huber (19). The geometry of hadacidin was based on a related structural fragment (20), retrieved by a search of the Cambridge Data Base. Models of hadacidin with a planar nitrogen and with tetrahedral nitrogens in L- and D-configurations were refined individually. In early rounds of refinement, both crystal structures were heated

Table I

Refinement statistics for adenylosuccinate synthetase.

	$P3_221$ (298 K)	$P3_221$ (100 K)
Resolution limit (Å)	2.8	2.5
Number of measurements	156,061	161,473
Number of unique reflections	16,429	22,201
Completeness of data set (%)	98	98
Completeness of data in the last resolution shell (%)	95 (2.90-2.80 Å)	96 (2.61-2.50 Å)
R_{sym}[a]	9.7	7.9
Number of reflections in refinement[b]	12,221	19,932
Number of atoms[c]	4,622	5,516
Number of solvent sites	156	454
R-factor[d]	0.171	0.206
R-free[e]	0.250	0.255
Resolution (Å)	5 to 2.8	5 to 2.5
Mean B ($Å^2$) for protein	26	17
Root mean square deviations		
Bond lengths (Å)	0.016	0.013
Bond angles (deg)	2.01	1.89
Dihedral angles (deg)	24.7	24.8
Improper dihedral angles (deg)	1.61	1.63

[a] $R_{sym} = \Sigma_j\Sigma_i|I_{ij} - \langle I_j\rangle|/\Sigma_i\Sigma_j I_{ij}$, where i runs over multiple observations of the same intensity and j runs over all crystallographically unique intensities. [b] All data in the resolution ranges indicated. [c] Includes hydrogens linked to polar atoms. [d] $R_{factor} = \Sigma||F_{obs}| - |F_{calc}||/\Sigma|F_{obs}|$, $|F_{obs}| > 0$. [e] R_{factor} based upon 10% of the data randomly culled and not used in the refinement.

to 2000 K and then cooled in steps of 25-300 K. In later rounds of refinement, the systems were heated to 1000 or 1500 K but then cooled in steps of 10 K. After the slow cooling protocol was completed (at 300 K), the models were subjected to 120 steps of conjugate gradient minimization, followed by 20 steps of individual B-parameter refinement. Individual B-parameters were subject to the following restraints: nearest neighbor, main side chain atoms, 1.5 $Å^2$; next to nearest neighbor, main chain atoms, 2.0 $Å^2$; nearest neighbor,

chain atoms, 2.0 $Å^2$; and next to nearest neighbor, side chain atoms, 2.5 $Å^2$.

Water molecules were added if (i) electron density at a level of 2.5σ was present in maps based on Fourier coefficients $(F_{obs} - F_{calc})e_i^{\alpha calc}$ and $(2F_{obs} - F_{calc})e_i^{\alpha calc}$, and (ii) acceptable hydrogen bonds could be made to an existing atom of the model. If after refinement a site for a water molecule fell beyond 3.3 Å from its nearest neighbor, that site was omitted from the model. In addition, water molecules were deleted from the model if their thermal parameters exceeded 80 $Å^2$. Harmonic restraints (50 kcal/mol) were placed on the positions of oxygen atoms of the water molecules to allow new water molecules to relax by adjustments in orientation. Occupancies of water molecules were not refined because of the high correlation between occupancy and thermal parameters for data of 2.6 Å nominal resolution. Thus solvent sites with B values between 50 and 80 $Å^2$ probably represent water molecules with occupancy parameters below 1.0 and thermal parameters substantially lower than those reported from the refinement.

Results

Quality of the Refined Models – The model reported here has been deposited with the Protein Data bank, Brookhaven National Laboratory (code 1NHT). The method of Luzzati (21) indicates an uncertainty in coordinates of 0.30 Å. The amino acid sequence used in refinement is identical to that reported by Silva *et. al.* (15). Results of the refinement are in Table I.

The Ramachandran plot (22) for the structures reported here are comparable with those of Poland *et. al.* (1). As in other crystal forms of the synthetase (1,15,23-25), the most apparent outlier is Gln-10, which exists in the same conformation in each of the five

independent polypeptide chains of three crystal forms. The program PROCHECK (26) indicates better stereochemistry for both the low and room temperature models than is typical for a structure of 2.5 Å resolution. The low temperature data set is superior in nominal resolution ($\langle I \rangle = 2\sigma(I)$ at 2.6 Å relative to 3.1 Å for the room temperature data). A much improved electron density map is the most significant consequence of the superior data acquired at low temperature. We observed no significant divergence between the room temperature and low temperature structures.

The average thermal parameter in the low temperature model varies from 5-33 $Å^2$ for atoms of the main chain and 5-37 $Å^2$ for atoms of side chains. The corresponding variations for the room-temperature structure are 14-43 and 14-44 $Å^2$, respectively, for main and side chain atoms. The variation in average thermal parameter as a function of residue number for the structures reported here are comparable with those of the IMP/NO_3^- complex (1).

Ligand Binding Sites – The complex of 6-thiophosphoryl-IMP, GDP, Mg^{2+}, and hadacidin (Fig. 1) is isomorphous to that of IMP, GDP, NO_3^-, Mg^{2+}, and hadacidin (1) and to that of hydantocidin 5'-phosphate, GDP, HPO_4^{2-}, Mg^{2+}, and hadacidin (25). A view of one monomer of the synthetase dimer with associated ligands appears in Fig. 2. Conformational changes in the synthetase upon ligation are described by Poland *et. al.* (1) as are the interactions of GDP, Mg^{2+}, and hadacidin, which are the same here within experimental error. Fig. 3 is a pictorial summary of the important interactions of ligands in the active site of the synthetase.

We focus, then, on the one feature that sets the present work apart from the former studies. The IMP and NO_3^- sites are connected by continuous electron density, which we can interpret only as a molecule of 6-thiophosphoryl-IMP (Fig. 4). Omit maps are generated

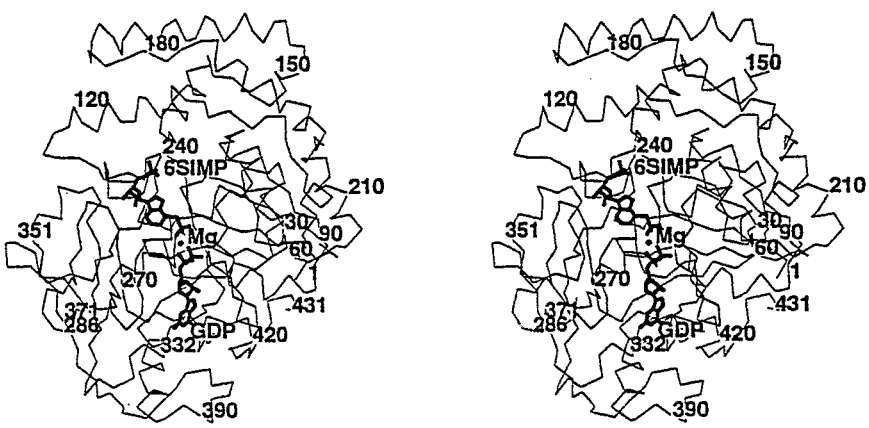

Figure 2. Stereoview of bound ligands in relation to a trace of α-carbons of adenylosuccinate synthetase.

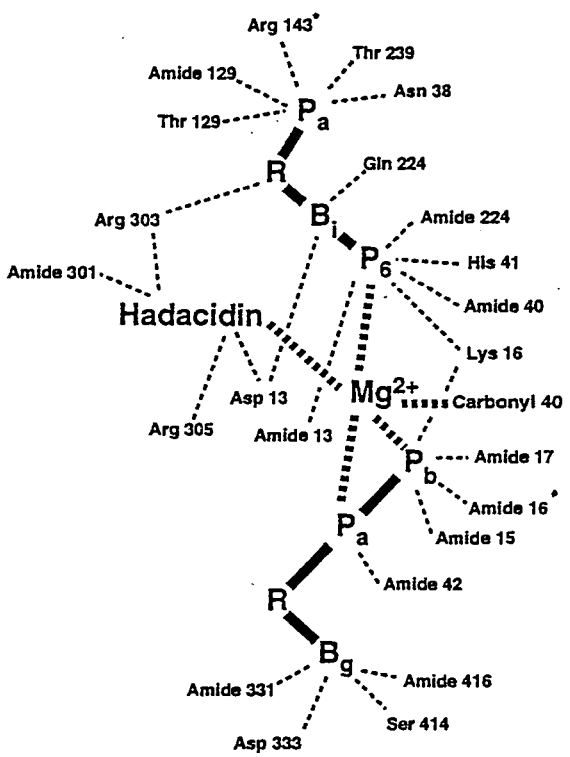

Figure 3. Diagram of selected hydrogen and coordinate bonding of ligands in the active site of adenylosuccinate synthetase. *R*, ribose; P_a, α-phosphate; P_6, 6-phosphoryl group; B_i, base of IMP; B_g, base of GDP.

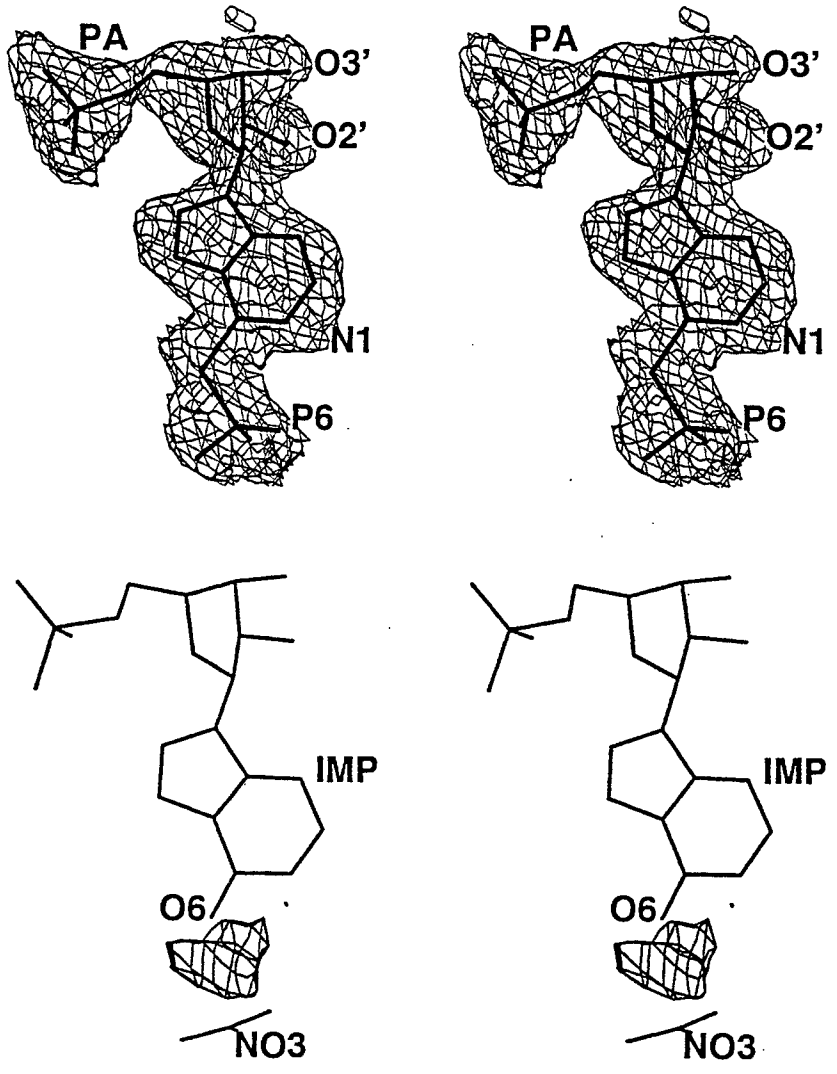

Figure 4. Electron density associated with 6-thiophosphoryl-IMP from a $2F_{obs} - F_{calc}$ map (*top*). Difference map based on observed data from the 6-phosphoryl-IMP complex and the IMP/NO_3^- complex (1), using calculated phases from the IMP/NO_3^- complex (*bottom*). Contour levels for both maps is 6-σ, with a cover radius of 1.0 Å employed in the *top* illustration.

from coefficients $2F_{obs} - F_{calc}$. Thermal parameters of atoms of 6-thiophosphoryl-IMP are comparable with those of the surrounding protein, suggesting full occupancy of the ligand. Thus, the electron density between the 6-sulfur and the phosphoryl group cannot arise as a consequence of the mutually exclusive binding of phosphate and 6-mercapto-IMP, with each ligand in partial occupancy. Finally, a model for 6-thio-phosphoryl-IMP fits the electron density well, leaving behind no significant density in difference maps. Indeed, a difference map, based on observed data from the IMP/NO_3^- and 6-thio-phosphoryl-IMP complexes and calculated phase angles from the IMP/NO_3^- complex, reveals a strong and well defined peak of electron density in the area between the 6-oxygen of IMP and the nitrogen of NO_3^- (Fig. 4).

Interactions involving the 5'-phosphate, the ribose, and the base (exclusive of the 6-thiophosphoryl group) of the 6-thiophosphoryl-IMP are the same as those of IMP in an earlier study (1). The 5'-phosphate hydrogen bonds with OG1 of Thr-129, backbone amide 129, ND2 of Asn-38, OG1 of Thr-239, and the guanidinium group of Arg-143 of the symmetry related monomer (Table II). In addition, three water molecules, 554, 636, and 732, mediate interactions between the 5'-phosphate and the protein. The 5'-phosphate of the 6-thiophosphoryl-IMP along with the side chain of Asp-114 (conserved in all known sequences of the synthetase) lie at the N terminus of helix H4. No direct hydrogen bonds, however, exist between helix H4 and either Asp-114 or the 5'-phosphate.

The 2'-OH group of the ribose of 6-thiophosphoryl-IMP hydrogen bonds with the guanidinium of Arg-303 and the 2'-OH hydrogen bonds with waters 524 and 699, which in turn interact with backbone carbonyls 126 and 273, respectively. Although the data are not of sufficient resolution to unambiguously determine the state of puckering of the ribose, the

Table II

Selected contacts (less than 3.4 Å) involving 6-thiophosphoryl-IMP.

Ligand atom	Contact atom	Distance (Å)
N1	OD1 Asp-13	2.94
N7	NE2 Gln-224	2.66
S6	NE2 Gln-224	2.94
O2'	NH2 Arg-303	2.63
	O Val-273	2.87
O3'	OW Wat-699	2.93
	OW Wat-524	3.08
O1A	N Thr-129	2.93
	OG1 Thr-129	2.68
	OW Wat-554	3.14
O2A	NH1 Arg-143[a]	3.17
	OW Wat-732	2.60
O3A	ND2 Asn-38	2.90
	OG1 Thr-239	2.51
	OW Wat-554	3.14
O2	N Asp-13	2.58
	NZ Lys-16	2.79
O1	NZ Lys-16	2.72
	NE2 His-41	3.27
	N Gln-224	2.70
O3	Mg^{2+}	2.17
	O1B GDP	2.61
	N Gly-40	3.24

[a] Symmetry-related subunit.

best fit to the electron density occurs with a low energy 2'-*endo* conformation (pseudorotation phase angle, 166°). The torsion angles O5'-C5'-C4'-C3' (γ by convention) and O4'-C1'-N9-C4 (χ by convention) are 44° (+*synclinal*) and -135° (*anti*), respectively.

The base of 6-thiophosphoryl-IMP interacts with the amide side chain of Gln-224 through its N7 and S6 atoms and with the side chain of Asp-13 through its N1 position. Interactions of 6-thiophosphoryl-IMP are dominated by the 6-thiophosphoryl group. Backbone amides 13, 40, and 224, NZ of Lys-16, NE2 of His-41, and NE2 of Gln-224 hydrogen bond with oxygen and sulfur atoms of the thiophosphoryl group (Fig. 5). In

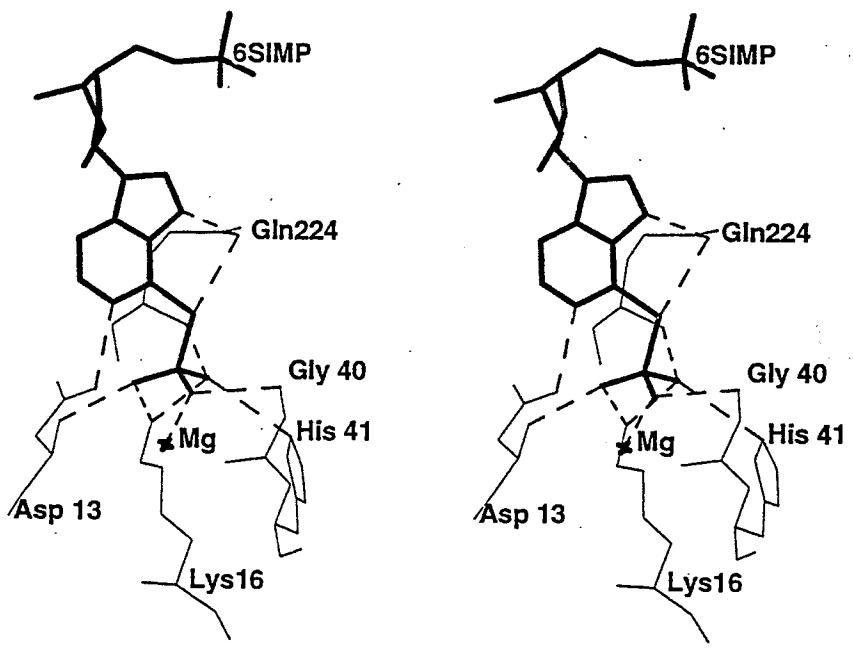

Figure 5. Stereoview of 6-thiophosphoryl-IMP in the active site of the ligated synthetase at 100 K, showing interactions of the base and 6-thiophosphoryl group. *Dashed lines* represent donor-acceptor interactions less than 3.2 Å. The 6-phosphoryl intermediate is drawn with *bold lines.*

addition, one of the oxygens of the thiophosphoryl group coordinates to the Mg^{2+}. The oxygen atoms of the thiophosphoryl group correspond in position to the oxygens of NO_3^- in the IMP/NO_3^- complex (1) and to three of four oxygens of HPO_4^{2-} in the hydantocidin 5'-phosphate complex (25). His-41 interacts with the β-phosphate of GDP when NO_3^- resides in the phosphoryl site, as observed in the IMP/NO_3^- complex (1). In the hydantocidin 5'-phosphate complex (25), which has HPO_4^{2-} at the phosphoryl site, His-41 interacts with the HPO_4^{2-} molecule, similar to the interaction observed for His-41 here. Presumably the increase in formal electrostatic charge from –1 to –2 is responsible for the interaction of His-41 with the anion located in the phosphoryl site.

Discussion

Markham and Reed (8) deduced a ΔG of +5 kcal/mol at pH 7 for the reaction GTP + 6-thiophosphoryl-IMP + L-aspartate ↔ GDP + thiophosphate + adenylosuccinate. Even in the absence of hadacidin, which leads to the dead end kinetic complex observed here, the combination of GTP, 6-mercapto-IMP, aspartate, Mg^{2+}, and enzyme should lead to undetectable levels of product. A plausible outcome of the crystallization of GTP, 6-mercapto-IMP, Mg^{2+}, and hadacidin, then, would be a 6-mercapto-IMP-GTP or 6-mercapto-IMP-GDP complex. The ratio of GDP to GTP in the active site would depend largely on the rate of hydrolysis of GTP in the bulk solvent and the rate of exchange of guanine nucleotides between the active site and the bulk solvent. Instead, the active site contains 6-thiophosphoryl-IMP and GDP. The presence of 6-thiophosphoryl-IMP in the active site indicates a lower free energy for the 6-thiophosphoryl-IMP/enzyme complex than for the substrate/enzyme complex. Thus, the enzyme must be a thermodynamic trap for the 6-

thiophosphoryl intermediate.

Several factors favor the formation of 6-thiophosphoryl-IMP in the active site of the synthetase. First, the pK_a of N1 of the 6-mercapto-IMP is approximately 1-1.5 pH units lower than that of N1 of IMP. Thus, Asp-13, which is a putative catalytic base in the abstraction of the proton from N1 of IMP (1), may be more effective in stabilizing the ionized form of the 6-mercapto nucleotide relative to the 6-oxo nucleotide (Fig. 6). In addition, the S-P thioester bond (approximately 2.1 Å in length) is 0.5 Å longer than the O-P ester bond. The increased bond length allows the three oxygens of the 6-thiophosphoryl group to occupy the positions of oxygen atoms of NO_3^- in the IMP/NO_3^- complex (1). Markham and Reed (6) have shown synergy in the binding of IMP, GDP, Mg^{2+}, and NO_3^- to the synthetase. The distance between N of NO_3^- and the 6-oxygen of IMP in the IMP/NO_3^- complex is 2.7 Å, implying a strong electrostatic interaction between an electron deficient N of NO_3^- and an electron-rich 6-oxygen of IMP (1). In the present study, the 6-sulfur (presumably stabilized initially as a thioanion) and the phosphorus atom of PO_3^- (putatively derived from the γ-phosphate of GTP and stabilized in the NO_3^- site) form a covalent bond as a consequence of electrostatic interactions and the increased atomic radii of sulfur and phosphorus relative to oxygen and nitrogen.

The proposed mechanism for the formation of the 6-thio-phosphoryl-IMP in the active site appears in Fig. 6. The interaction involving Asp-13 identifies it as a possible catalytic base in the abstraction of the proton from N1 of 6-mercapto-IMP and generation of a 6-thioanion. In fact, the natural substrate IMP may be in the 6-oxyanion state, when bound to the active site. Gln-224 may stabilize the 6-thioanion further by a hydrogen bond interaction. Mutation of Asp-13 to alanine inactivates the synthetase completely (27), and

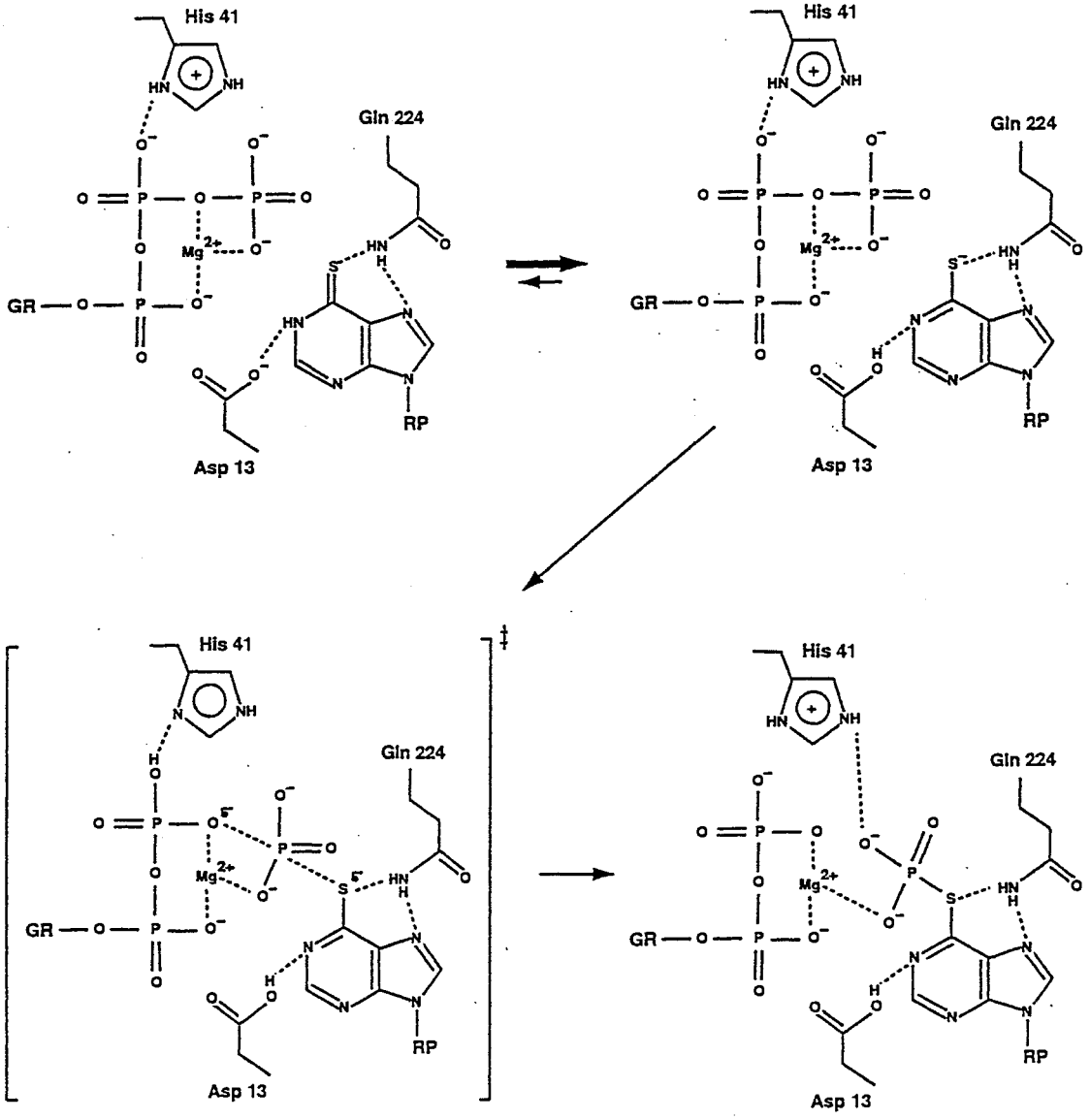

Figure 6. Proposed mechanism for the phosphotransfer reaction governed by the synthetase, involving 6-mercapto-IMP as a substrate. L-Aspartate is not shown here but is putatively coordinated to Mg^{2+} as shown in Fig. 7.

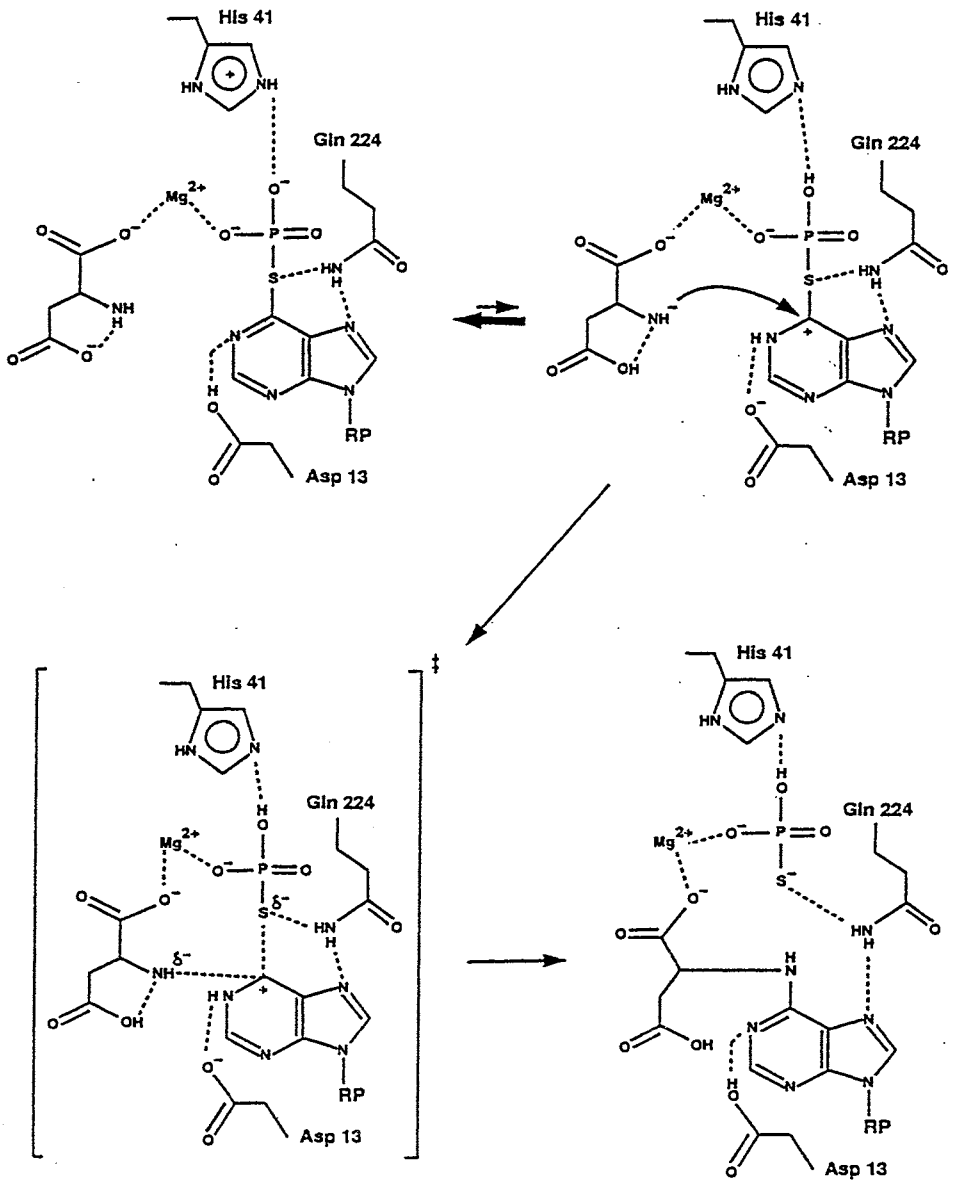

Figure 7. Proposed mechanism for the displacement of thiophosphate from 6-thiophosphoryl-IMP by aspartate. GDP is not shown here but remains coordinated to Mg^{2+} through its α- and β-phosphates, as depicted in Fig. 6.

mutation of the Gln-224 to glutamate reduces k_{cat} by 1000-fold at pH 7.7. The interaction involving Gln-224 is relevant to reported differences in the recognition of IMP analogs by the synthetase from mammals and leishmanial parasites (28,29). Allopurinol ribonucleotide, which differs from IMP at position 7 of the purine ring system, is not recognized as a substrate by mammalian adenylosuccinate synthetase but is a poor substrate for the synthetase from leishmanial parasites. As Gln-224 alone recognizes N7 of IMP, the equivalent position in the synthetases from other organisms may be an important determinant of substrate specificity. Unfortunately, the sequence of the synthetase from a leishmanial parasite is not available.

The 6-thioanion then displaces GDP from the γ-phosphate of bound GTP (Fig. 6). Both His-41 and Mg^{2+} probably play important roles in stabilizing charge development on the β- and γ-phosphates of GTP in the transition state (1). A His-41 to asparagine mutant is inactive (27) and Mg^{2+} is required for activity of the synthetase (10).

The second reaction governed by the synthetase involves the nucleophilic displacement of thiophosphate from the 6-phosphoryl intermediate by the amino group of L-aspartate (Fig. 7). The conformation and interactions of aspartate are inferred from enzyme-bound hadacidin (1). The putative conformation of bound aspartate favors a hydrogen bond between its β-carboxylate in abstracting a proton from that amino group. No direct evidence is available regarding the catalytic role of the β-carboxylate of aspartate. However, an α-amino acid is a substrate of the synthetase only if it bears a negatively charged substituent with carboxylate-like geometry at the β-carbon (30). Hydroxylamine may not require the catalytic support of the β-carboxylate because the pK_a of its amine is significantly lower than

that of the α-amino group of aspartate.

Assuming a catalytic function for the β-carboxylate of aspartate (there are no other candidates provided by the enzyme (1)), a total of three hydrogen bonds, then, may be involved in promoting the second reaction: (i) the putative interaction between the α-amino and β-carboxylate groups of aspartate, (ii) the hydrogen bond between Asp-13 and N1 of the phosphoryl intermediate, and (iii) the hydrogen bond between His-41 and the 6-phosphoryl group. The first interaction enhances the nucleophilicity of C6 of the intermediate, and the third hydrogen bond stabilizes the developing charge on the leaving group (thiophosphate in this case). The extent to which these three hydrogen bonds promote catalysis in the second reaction cannot be answered on the basis of the present study.

Poland *et. al.* (1) suggest a more significant interaction between Asp-13 and Mg^{2+} after formation of the phosphoryl intermediate, hence transforming Asp-13 from a catalytic base in the phosphotransfer step into a catalytic acid for the second reaction. In the present complex, we observe no significant movement of Asp-13 toward the Mg^{2+}. Coordinate uncertainty (0.3 Å), however, could obscure small but catalytically significant changes in the distance of Asp-13 to Mg^{2+}.

Lieberman (10) was the first to propose the formation of 6-phosphoryl-IMP as an intermediate on the reaction pathway governed by the synthetase, but the results of his study are consistent with two other proposed mechanisms (3). Miller and Buchannan (31) suggest as attack of aspartate on C6 of IMP in concert with an attack by the 6-oxygen of IMP on the γ-phosphate of GTP. Markham and Reed (7) were unable to find spectral evidence for the formation of a 6-phosphoryl intermediate and, as a consequence, suggested that the addition of aspartate to C6 of IMP preceded the phosphorylation of O6. Isotope exchange studies at

equilibrium by Cooper *et. al.* (13), however, support the formation of 6-phosphoryl-IMP prior to the nucleophilic attack of aspartate. Furthermore, Bass *et. al.* (12) demonstrated the chemical exchange of ^{18}O from the β,γ-bridging position of GTP to the oxygens of the β-phosphate of GTP in the presence of enzyme and IMP or in the presence of enzyme, IMP, and succinate (as an analog of aspartate). Isotope exchange could only occur if the γ-phosphate dissociates from GTP for an interval long enough to allow the rotational isomerization of the β-phosphate group. The absence of labeled phosphate in solution demonstrated that the dissociated γ-phosphate remained bound to the enzyme. As IMP was required for isotope exchange, Bass *et. al.* (12) suggested that the dissociated γ-phosphate existed as 6-phosphoryl-IMP. The observation here of 6-thiophosphoryl-IMP in the active site of the synthetase is entirely consistent with the results and conclusions of the isotope exchange studies.

Acknowledgements

We thank Drs. Fred Rudolph and Bruce Cooper for their generous gift of hadacidin.

References

1. Poland, B. W., Fromm, H. J. & Honzatko, R. B. (1996) *J. Mol. Biol.* **264**, 1013-1027.
2. De Abreu, R. A. (1995) in *Purine and Pyrimidine Metabolism in Man VIII* (Sahota, A. & Taylor, M., eds) pp. 195-200, Plenum Publishing Corp., New York.
3. Stayton, M. M., Rudolph, F. B., & Fromm, H. J. (1983) *Curr. Top. Cell. Regul.* **22**, 103-141.
4. Rudolph, F. B. & Fromm, H. J. (1969) *J. Biol. Chem.* **244**, 3832-3839.

5. Clark, S. W. & Rudolph, F. B. (1976) *Biochim. Biophys. Acta* **437**, 87-93.

6. Markham, G. D. & Reed, G. H. (1977) *Arch. Biochem. Biophys.* **184**, 24-35.

7. Markham, G. D. & Reed, G. H. (1978) *J. Biol. Chem.* **253**, 6184-6189.

8. Kaczka, E. A., Gitterman, C. O., Dulaney, E. L. & Folkers, K. (1962) *Biochemistry* **1**, 340-343.

9. Shigeura, H. T. (1967) in *Antibiotics* (Gottieb, D. & Shaw, P., eds) pp. 451-456, Springer-Verlag New York Inc., New York.

10. Lieberman, I. (1956) *J. Biol. Chem.* **223**, 327-339.

11. Fromm, H. J. (1958) *Biochim. Biophys. Acta* **29**, 255-262.

12. Bass, M. B., Fromm, H. J. & Rudolph F. B. (1984) *J. Biol. Chem.* **259**, 12330-12333.

13. Cooper, B. F., Fromm, H. J. & Rudolph, F. B. (1986) *Biochemistry* **25**, 7323-7327.

14. Bass, M. B., Fromm, H. J. & Stayton, M. M. (1987) *Arch. Biochem. Biophys.* **256**, 335-342.

15. Silva, M. M., Poland, B. W., Hoffman, C. R., Fromm, H. J. & Honzatko, R. B. (1995) *J. Mol. Biol.* **254**, 431-446.

16. Howard, A. J., Nielsen, C. & Xuong, N. H. (1985) *Methods Enzymol.* **114**, 452-472.

17. Cambillau, C. & Horjales, E. (1987) *J. Mol. Graphics* **5**, 174-177.

18. Brünger, A. T. (1992) *XPLOR*, Version 3.1., Yale University Press, New Haven, CT.

19. Engh, R. A. & Huber, R. (1991) *Acta. Crystallogr. Sec. A* **47**, 392-400.

20. Bernardinelli, G., Tronchet, J. M. J. & Bizzozero, N. (1991) *Z. Kristallog.* **195**, 135-138.

21. Luzzati, V. (1952) *Acta. Crystallogr.* **5**, 802-810.

22. Ramachandran, G. N., Ramakrishnan, C. & Sasisekharan, V. (1963) *J. Mol. Biol.* **7**, 95-99.

23. Poland, B. W., Silva, M. M., Serra, M. A., Cho, Y., Kim, K. H., Harris, E. M. S. & Honzatko, R. B. (1993) *J. Biol. Chem.* **268**, 25334-25342.

24. Poland, B. W., Hou, Z., Bruns, C., Fromm, H. J. & Honzatko, R. B. (1996) *J. Biol. Chem.* **271**, 15407-15413.

25. Poland, B. W., Lee, S.-F., Subramanian, M. V., Siehl, D. L., Anderson, R. J., Fromm, H. J. & Honzatko, R. B. (1996) *Biochemistry* **35**, 15753-15759.

26. Laskowski, R. A., Mac Arthur, M. W., Moss, D. S. & Thornton, J. M. (1993) *J. Appl. Crystallogr.* **26**, 283-291.

27. Kang, C., Poland, B. W., Gorrell, A., Honzatko, R. B. & Fromm, H. J. (1997) *J. Biol. Chem.* **272**, 11881-11885.

28. Spector, T., Jones, T. E. & Elion, G. B. (1979) *J. Biol. Chem.* **254**, 8422-8426.

29. Spector, T., Berens, R. L. & Marr, J. J. (1982) *Biochem. Pharmacol.* **31**, 225-229.

30. Porter, D. J. T., Rudie, N. G. & Bright, H. J. (1983) *Arch. Biochem. Biophys.* **225**, 157-163.

31. Miller, R. W. & Buchanan, J. M. (1962) *J. Biol. Chem.* **237**, 485-490.